PROCEEDINGS A

rspa.royalsocietypublishing.org

Review

Article submitted to journal

Subject Areas:
Convection, Flow in porous media

Keywords:
xxxx, xxxx, xxxx

Author for correspondence:
Duncan Hewitt
e-mail: d.hewitt@ucl.ac.uk

Vigorous convection in porous media

D. R. Hewitt

Department of Mathematics, University College London, UK

The problem of convection in a fluid-saturated porous medium is reviewed with a focus on 'vigorous' convective flow, when the driving buoyancy forces are large relative to any dissipative forces in the system. This limit of strong convection is applicable in numerous settings in geophysics and beyond, including geothermal circulation, thermohaline mixing in the subsurface, and heat transport through the lithosphere. Its manifestations range from 'black smoker' chimneys at mid-ocean ridges to salt-desert patterns to astrological plumes, and it has received a great deal of recent attention because of its important role in the long-term stability of geologically sequestered CO_2. In this review, the basic mathematical framework for convection in porous media governed by Darcy's law is outlined, and its validity and limitations discussed. The main focus of the review is split between 'two-sided' and 'one-sided' systems: the former mimics the classical Rayleigh–Bénard setup of a cell heated from below and cooled from above, allowing for detailed examination of convective dynamics and fluxes; the latter involves convection from one boundary only, which evolves in time through a series of regimes. Both setups are reviewed, accounting for theoretical, numerical and experimental studies in each case, and studies that incorporate additional physical effects are discussed. Future research in this area and various associated modelling challenges are also discussed.

THE ROYAL SOCIETY
PUBLISHING

1. Introduction

Convection - that is, the motion of fluid due to gravity acting on an unstable density profile - is a fundamental physical process that has motivated a wealth of academic research. It occurs across a wide range of contexts and scales, and plays a central role in a huge number of environmental processes.

This review is focussed on convection of fluid through porous media, which is a particularly important facet of geophysical fluid mechanics. Geothermal circulation of fluid through porous rock controls the mineralogy and heat transport in volcanic systems [1], while heat from deep within the Earth drives underground hydrothermal convection that is crucial for the extraction of geothermal energy [2]. Convective currents in both the continental and the oceanic lithosphere play a major role in the heat budget of the Earth [3–5]. The hydrology of mid-ocean ridges is controlled by strong porous convection and complex geochemistry, leading to convoluted flow structures, supersaturated saline plumes and distinctive rock morphologies including black and white 'smoker' chimneys [6]. Gradients in salt concentration can also lead to porous convection: surface evaporation drives the flow and migration of saline groundwater [7,8]; underwater salt domes drive local thermohaline circulation, affecting sediment transport oceanic mixing [9]; and salinity-driven convection through porous sea ice drives a salt flux into the ocean that plays a key role in global oceanic circulation [10]. Away from the Earth, strong porous convection is believed to drive hydrothermal currents on ice-covered moons of Saturn and Jupiter [11]. In all these situations, convection results in an enhancement of energy or solute transport and an enhancement of fluid mixing; the aim of studying convection is to better understand these processes.

In recent years, there has been particular renewed interest in porous convection because of its relevance for understanding the long-term fate of geologically stored carbon dioxide [12–16]. which has been widely discussed as a means of stabilizing rising atmospheric CO_2 levels [17]. Geological sequestration is achieved by injecting supercritical CO_2 deep underground into water-saturated porous rock formations. Supercritical CO_2, like oil and natural gas which are often found naturally in such formations, is buoyant relative to water, and so will rise after injection until it spreads below the impermeable caprock of the formation or continues to leak up to the surface. One mechanism that stabilizes injected CO_2 and avoids its potential leakage back into the atmosphere is its weak dissolution in the underlying water. Dissolution increases the density of the water and so can lead to downwelling convection, which, in turn, substantially increases the rate of dissolution of CO_2 at the water-CO_2 interface. This convective dissolution process has inspired a great deal of academic study over the last $10-15$ years; indeed, this wealth of recent research is one of the primary motivations for this review.

The basic process of convection is frequently encountered in everyday life, and its essential physics can be understood by considering the simple example of a pan of water heated on a hot plate (see also excellent expositions of the physics of convection in [18,19]) Water is heated by conduction (diffusion) through the base of the pan, which gradually warms up the water there while the fluid above remains colder. The additional energy given to water molecules as they are heated causes an increase in their mean free path, and thus in their volume, and so the water density decreases. This process leads to the formation of a density stratification, with less dense warm water lying below denser cold water. Such a stratification is, generically, unstable: if a parcel of fluid is raised slightly, it will experience a weaker downwards buoyancy force than its neighbours and will continue to rise. The fluid motion that ensues is called convection. An important feature of convective flow is that it can substantially enhance the transport, or flux, of buoyancy into the system. In the example of a heated pan, convection drives warmer water up and colder water down, and this replenishing of cold water near the base of the pan means that the temperature gradient between the hot plate and the water is much steeper than it would have been without convection. Thus, although all the heat entering the pan is conducted, the transport of heat can be greatly enhanced because of the action of convection.

Not all adverse density gradients lead to convection: the dissipative action of fluid viscosity and diffusion of temperature or solute act to inhibit convective motion. In a given situation, a comparison of the strength of the buoyancy forces with these dissipative effects gives rise to a dimensionless ratio known as the Rayleigh number, Ra (defined more fully in the following section). If the Rayleigh number is small, dissipative forces act to inhibit convection, whereas if it is large, buoyancy forces dominate and drive strong convective flow. One can equivalently think of the Rayleigh number as a comparison of timescales, given by the ratio of the time it would take for a patch of buoyancy to diffuse a characteristic distance H to the time it would take to transport the buoyancy that distance by convection. Large values of Ra thus describe situations in which convective motion is much faster than diffusive buoyancy transport. In a 'usual' unconfined fluid (*i.e.* not in a porous medium), large values of Ra lead to complex, highly turbulent dynamics. In a fluid-saturated porous medium, however, the physics of high-Ra convection are somewhat different, and that limit is the focus of this review.

Flow in a porous medium differs fundamentally from the flow of an unconfined fluid because it is controlled by viscous drag between the fluid and the porous matrix, as described by the permeability of the medium. As such, canonical porous flow is slow and inertia-free, and at a continuum or macroscopic scale the mean flow that is forced through the (microscopic) pores can be linearly related to the driving pressure gradients and buoyancy forces via 'Darcy's law'. There is no inertia or turbulence in such a flow, and for a given pressure and density the flow field is determined instantaneously. The complexity in these flows arises because density is transported by advection and diffusion, which gives rise to both time-dependence and non-linearity in the system. Indeed, while it can seem strange to consider the limit of 'vigorous' high-Ra convection when the flow is dominated by viscous drag, we will find that sufficiently strong buoyancy forces can still give rise to a rich variety of multi-scale, non-linear, spatio-temporally chaotic and 'vigorous' dynamics. Indeed, the essential mechanism of convection is the same as in an unconfined fluid: horizontal gradients in the buoyancy force generate local rotational flow, which act to drive less dense fluid up and more dense fluid down.

Historically, most studies of convection in porous media have focussed on questions of how and when convective flow is initiated, and how it subsequently evolves; until relatively recently, there was little focus on the behaviour of convective systems when the buoyancy forces are large (i.e. large Rayleigh number). This is in part because dissipative forces are inherently much larger in a porous medium than they are in an unconfined fluid: viscous drag from the pore scale always affects the flow at much larger scales. Typical velocity scales in porous media are thus much smaller than in an unconfined fluid; convective timescales are therefore longer and the Rayleigh number, which, as noted above, describes a ratio of diffusive and convective timescales, is typically much smaller than in an unconfined fluid. Nevertheless it can still be much larger than unity, and in many physical situations it is. The aim of this review is to provide an overview of recent advances in our understanding of this limit of high-Ra 'vigorous' convection in porous media. For a broader review of the topic of convection in porous media, the reader is referred to the book by Nield and Bejan [20], which provides a comprehensive overview of the subject and is now running in its fifth edition.

It is worth noting that in an unconfined fluid, the study of high-Ra convection has a long and interesting history (e.g. [18,19,21,22]). In particular, the quest to understand how the enhanced buoyancy transport associated with convection (the convective flux) depends on the governing parameters, as described in part by the Rayleigh number, has been an alluring and enduring one. It has produced a number of simple but very powerful concepts related to the behaviour and self-organisation of strong non-linear convective flows (e.g. the famous boundary-layer arguments of Malkus and Howard) as well as sophisticated mathematical bounding techniques and increasingly detailed experiments and numerical computations. Many of these ideas carry across to the case of convection in a porous medium, as we shall see. Indeed, from a theoretical standpoint, the relative simplicity of the equations governing idealised flow in a porous medium lead to a somewhat more tractable system for the study of convective dynamics and pattern

formation than in an unconfined fluid, allowing for more definitive progress in our understanding of high-Ra convection.

Of course, models describing flow in a porous medium rely on various assumptions which, in reality, can break down. Darcy's law, for example, becomes inaccurate if fluid moves through the pores of the matrix sufficiently rapidly that inertial forces can no longer be neglected compared to the viscous drag, while the parameterization of the medium's resistance to flow in terms of a single homogeneous permeability may be woefully inaccurate if the medium has a complex pore structure. Thus, while the main focus of this review is on the most idealised continuum models of flow in porous media, the various assumptions of these models and the manner in which they can break down is also discussed. Accounting for these assumptions, and understanding the role of various 'non-ideal' effects on convective flow through porous media, are areas of active research.

This review is structured around two canonical 'natural' convection problems (that is, problems in which convection is unforced by external flow), which are here denoted 'two-sided' and 'one-sided' systems. In this terminology, two-sided systems (§3) comprise a distributed buoyancy source on two boundaries (here always an upper and a lower boundary), such that the system evolves to a steady or quasi-steady state. This is the porous equivalent of the famous Rayleigh–Bénard cell, in which a rectangular domain is heated from below and cooled from above. For weak buoyancy forces (low Ra), this system provides a rich setting for the study of linear and non-linear stability and pattern formation, while for large Ra, which is the focus here, it allows for detailed study of convective buoyancy transport and the structures and unsteady dynamics of convection. One-sided systems (§4), in contrast, are here taken to mean systems driven by a distributed source along one boundary only, which evolve over time. They are, generally speaking, less convenient to the theorist for understanding convective dynamics, but rather more applicable to describe real systems. In each case, we begin with a description of the basic idealised system, and go on to discuss extensions to this problem that incorporate additional physics. Before this, the basic frameworks to model porous convection are outlined in §2, while a brief perspective on future directions for research in this area is presented in §5.

2. Mathematical modelling of convection in porous media

(a) Basic equations

The porosity ϕ of a porous medium is defined as the fraction of the medium that is made up of pore space. Continuum modelling of flow in porous media is typically achieved by taking the average of relevant quantities (pressure, density, velocity) in each pore over a representative volume that encapsulates many pores. As such, the flow is described in terms of the mean volume flux or Darcy velocity $\boldsymbol{u}$, which, assuming that the porosity ϕ is constant and the fluid is incompressible, satisfies

$$\boldsymbol{\nabla}\cdot\boldsymbol{u}=0. \tag{2.1}$$

In place of the Navier–Stokes equations for an unconfined fluid, in a porous medium the Darcy velocity $\boldsymbol{u}$ is governed by Darcy's law [23,24], which relates the driving pressure and buoyancy forces to the viscous drag imparted by the medium on the pore scale according to

$$\boldsymbol{u}=-\frac{k}{\mu}\left(\boldsymbol{\nabla}p-\rho\boldsymbol{g}\right), \tag{2.2}$$

where p and ρ are the fluid pressure and density, averaged over all the fluid in the representative volume, $\boldsymbol{g}$ the usual gravitational acceleration, μ the fluid viscosity and k the permeability of the medium. The permeability, which has dimensions of length squared and typically scales with the square of the mean pore size, is a critical parameter for flow in a porous medium: it is often modelled as a constant, but, more generally, depends on space and can be anisotropic (in which case it is replaced by a second-order tensor in (2.2)).

Convection occurs as a result of differences in the density ρ, which in most cases result from differences in the concentration C of a solute or on the temperature T of the fluid, or both. A

simple linear equation of state is often assumed,

$$\rho = \rho_0 \left(1 - \alpha_T T + \alpha_C C\right), \tag{2.3}$$

where $\alpha_T \geq 0$ and $\alpha_C \geq 0$ are the relevant coefficients of expansion or contraction associated with temperature or solute changes, and ρ_0 is a reference density.

In the case of solutal convection, the concentration field in the interstitial fluid evolves by advection and diffusion, as described by

$$\phi \frac{\partial C}{\partial t} + \boldsymbol{u} \cdot \boldsymbol{\nabla} C = \phi \nabla \cdot (D \nabla C), \tag{2.4}$$

where D is the effective solutal diffusivity in the medium (see discussion of dispersion in §2(d)ii below). In the case of thermal convection, one in general needs to consider conservation of heat in each phases of the porous medium [20]. Under the assumption that temperature is locally equilibrated between the phases, however, these equations reduce to

$$\overline{\phi} \frac{\partial T}{\partial t} + \boldsymbol{u} \cdot \boldsymbol{\nabla} T = \nabla \cdot (\kappa \nabla T), \tag{2.5}$$

where κ is the mean thermal diffusivity and $\overline{\phi} = \left[\phi \rho_l c_l + (1 - \phi) \rho_s c_s\right] / \rho_l c_l$ is a weighted average porosity in terms of the background density ρ_i and specific heat c_i of the liquid ($i = l$) or solid ($i = s$) phases. Equation (2.5) reduces to (2.4) on setting $c_s = 0$ and identifying $\kappa = \phi D$, and so, under the assumption of local thermal equilibrium, results for solutal convection can be equally interpreted as results for thermal convection, and vice-versa. One can alternatively relax the assumption of thermal equilibrium between the fluid and solid phases, by retaining individual, but coupled, temperature fields for each phase. Such 'non-equilibrium' models and their application to convection have been widely discussed in the literature (e.g. [25–27]), but not in the context of strong convection, and they are not considered here.

In the majority of studies of porous convection, including here, the (porous equivalent of the) Boussinesq, or Oberbeck–Boussinesq, approximation is assumed. That is, variations in density induced by temperature or solute are ignored everywhere except when multiplied by gravity in Darcy's law (thus, for example, density variations have a negligible effect on the fluid volume via conservation of mass, which instead reduces to the condition of incompressibility (2.1)). This approximation is usually held to be valid whenever variations in density $\Delta\rho$ from (2.3) are small relative to the magnitude of the density ρ_0 itself, which, in most physical situations of interest, is the case. [1]

(b) Buoyancy velocity and Rayleigh number

For a given density difference $\Delta\rho$, one can define the buoyancy velocity scale

$$\hat{u} = \Delta\rho \, g k / \mu, \tag{2.6}$$

which is the characteristic scale for convective motion of a parcel of fluid with a density difference $\Delta\rho$ from its neighbours. Note that, unlike in an unconfined fluid, the buoyancy velocity does not depend on the size of this parcel: convective structures of different sizes do not travel at different characteristic speeds in a porous medium. The ratio of the timescale to diffuse a distance H (that is, H^2/κ or $H^2/\phi D$) to the timescale to convect over that distance ($H/\hat{u}$) yields the key parameter

[1] In fact, the formal limit in which the Boussinesq approximation applies in a porous medium is somewhat more involved than simply $\Delta\rho \ll \rho_0$; see Landman and Schotting [28] for details. However, it remains the case that the approximation will be a good one in most cases for which $\Delta\rho \ll \rho_0$.

for convection, the Rayleigh number, defined here for either solutal or thermal convection,

$$Ra = \frac{\hat{u}H}{\phi D} = \frac{\Delta\rho\, g\, kH}{\phi D\mu} \qquad \text{or} \qquad Ra = \frac{\hat{u}H}{\kappa} = \frac{\Delta\rho\, g\, kH}{\kappa\mu}. \tag{2.7a, b}$$

Generally speaking, if the Rayleigh number is sufficiently small, the dissipative effects of diffusion and viscosity will inhibit any convective motion. Conversely, if Ra is large, the driving buoyancy forces dominate and we expect vigorous convection.

Note that the porous Rayleigh number (2.7) is related to the standard unconfined-fluid Rayleigh number $\mathcal{R}$ by a factor of k/H^2, which is often labelled the Darcy number Da, so that $Ra = Da\mathcal{R}$. The Darcy number is effectively the square of a dimensionless ratio between the microscopic pore scale $\delta_p \sim k^{1/2}$ and the macroscopic length scale H, and so is typically extremely small (*e.g.* a 100m-deep sandstone aquifer might have $k/H^2 \sim 10^{-14}$ or smaller). As such, porous Rayleigh numbers are much smaller than their unconfined equivalents, and the limit of 'large' Rayleigh number used in this review refers roughly to $Ra \gtrsim O(10^3)$.

In fact, the permeability provides one of the main constraints on the size of the Rayleigh number: permeability in rocks can vary by many orders of magnitude, and buoyancy transport in fine-grained low-permeability rock is unlikely to be convective. However, in many cases we are interested in convective flow through permeable sedimentary formations and aquifer rocks, and the Rayleigh number can be large. In geothermal volcanic systems, for example, temperature contrasts of $O(100^\circ\,\mathrm{C})$ over a kilometre could give Rayleigh numbers $Ra = O(10^4)$, while the Rayleigh number associated with convective dissolution of CO_2 in a permeable aquifer could be even larger, (in part because of the small molecular diffusivity of CO_2 in water). It is worth noting that even at very large Ra, the associated buoyancy velocity (2.6) can still be relatively slow (*e.g.* fractions of metres per day).

(c) The essential physics of porous convection

The basic mechanism of convective flow in a porous medium becomes clear upon taking the curl of Darcy's law (2.2). For the simplest case of a two-dimensional medium in the (x, z) plane with constant parameters, this operation yields

$$\Omega_y = \frac{kg}{\mu}\frac{\partial\rho}{\partial x}, \tag{2.8}$$

where $\Omega_y = w_x - u_z$ is the out-of-plane component of the vorticity vector. We can see that horizontal gradients in buoyancy drive rotational flow in the plane, with a magnitude determined by the buoyancy-velocity scale $\hat{u}$ (2.6). Sloped isopycnals thus drive convective motion (or, more generally, isopycnals with a normal vector that is not aligned with gravity). Convective instabilities of flat isopycnals result when the induced rotational flow associated with a small perturbation to the isopycnal slope is sufficiently strong to overcome the restoring action of diffusion. Note that this relationship is instantaneous: in the absence of inertia the flow reacts instantly to any changes in the density. The time dependence - and non-linear complexity - in the system comes from the evolution of the density field via advection and diffusion as described by (2.4) or (2.5).

The equivalent expression for the vorticity in three dimensions is

$$\boldsymbol{\Omega} = \frac{kg}{\mu}\left(-\frac{\partial\rho}{\partial y}, \frac{\partial\rho}{\partial x}, 0\right), \tag{2.9}$$

illustrating the same effect: rotations in the (y, z) and (x, z) planes are (instantaneously) driven by sloped isopycnals.

(d) Key modelling assumptions

(i) Heterogeneities and anisotropy

Real porous media are inevitably heterogeneous at some scale. In some cases, this heterogeneity might be sufficiently small-scale and statistically random that a single bulk permeability is a reasonable description of the medium, but in others, these variations may be macroscopic and can have a significant effect on flow. High-permeability lenses or low-permeability baffles in rocks, for example, can restrict the size of convective structures and channel flow in specific directions. It is straightforward to account for basic permeability variations in (2.2) by simply allowing the permeability to vary spatially, although the impact on the resultant dynamics may be very significant. Real media may also be anisotropic: there may be greater resistance to flow in certain directions than in others, as in media with a complex microstructure, like a dense fibrous suspension or a rock that has been substantially compressed along one axis. To incorporate anisotropy, the scalar permeability is replaced by a second-order tensor in (2.2).

More challenging for the modeller are situations in which the medium exhibits multiple scales of pore structure: a heavily fractured porous rock could be described in terms of a large-scale porosity and permeability, describing the fractures, and small-scale values describing the original pore space; similar bidispersity between a large and small scale of porosity or permeability can be found in various biological systems or fabricated industrial media. In these cases, one typically proceeds by introducing two 'phases' of pore-space, resulting in a substantially more complicated set of governing equations and associated parameters. Such models have been explored in the context of low and moderate Ra convection (e.g. [29–31]), but the limit of high-Ra convection in bi-disperse or dual-permeability media has not, to my knowledge, been considered.

(ii) Mechanical dispersion

In their simplest form, the thermal or solutal diffusivity in the equations governing the evolution of temperature and solute (2.4) - (2.5) are assumed to be constant. There is, however, an increasing understanding that hydrodynamic dispersion - that is, flow-induced mechanical dispersion through the pore structure of the medium - can provide a very significant enhancement to mixing in the presence of flow. As fluid percolates through a porous medium, individual fluid parcels are constantly changing direction as they navigate the microscopic pore structure. This results in a random-walk-style drift, which can typically be described as an enhanced velocity-dependent effective diffusivity. Dispersion is not isotropic: tracers will spread much further in the flow direction than in the transverse direction. Most dispersion models and experimental data suggest that dispersion in the presence of a flow u depends on the pore-scale Peclet number $Pe = u\delta_p/D$ (or $u\delta_p/\kappa$), where $\delta_p \sim k^{1/2}$ is the pore size (e.g. [32]): if Pe is $O(1)$ or smaller, dispersion is unimportant, but if Pe is greater than $O(10)$, the effective dispersion increases roughly linearly with Pe (see *e.g.* [33] and references therein).

(iii) Break-down of Darcy's law

Darcy's law (2.2) provides a simple relationship between the mean volume flux through a representative volume of pores and the driving pressure gradients. Its validity fundamentally relies on the fact that the lengthscales of flow structures remain large relative to the size of the representative volume over which one has averaged. One might be particularly worried about these assumptions in the context of vigorous high-Ra convection, where velocities can be relatively large and flow structures small. There are two key limits that need to be considered. First, Darcy's law requires that inertial terms are negligible relative to viscous drag on the pore-scale; *i.e.*, the pore-scale Reynolds number Re_p should be small, where $Re_p \sim \hat{u}\rho\delta_p/\mu \sim \hat{u}\rho k^{1/2}/\mu$, given that the typical pore size δ_p scales with the square root of the permeability; that is, we require

$$\hat{u}k^{1/2}\frac{\rho}{\mu} \ll 1 \qquad \text{or} \qquad \frac{RaDa^{1/2}}{Pr} \ll 1, \tag{2.10}$$

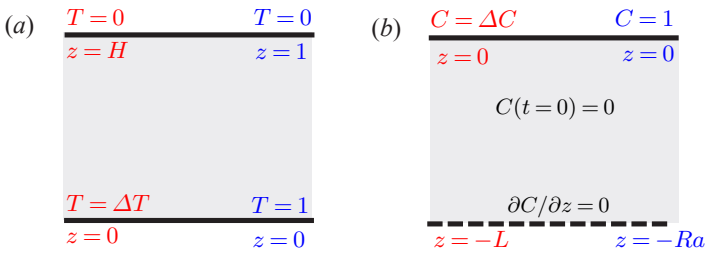

Figure 1. Simple schematics of (a) the 'two-sided' and (b) the 'one-sided' systems, shown in two dimensions with dimensional labels (red, left) and equivalent dimensionless labels (blue, right) according to the scalings discussed in the main text in each case.

written in terms of the Rayleigh number Ra (2.7), Darcy number $Da = k/H^2$ and Prandtl number $Pr = \mu/\rho\kappa$. Second, the length-scales of the convective flow must remain large relative to the scale of the pores. At high Ra, the smallest structures of the flow scale with the advection–diffusion lengthscale $\kappa/\hat{u}$ (or $D/\hat{u}$ for solutal convection), and comparison with the pore scale $\delta_p \sim k^{1/2}$ suggests that the validity of Darcy's law requires

$$\frac{\hat{u}k^{1/2}}{\kappa} \ll 1 \qquad \text{or} \qquad RaDa^{1/2} \ll 1. \tag{2.11}$$

In fact, this condition is the same as the condition $Pe \ll 1$ discussed in §ii above for mechanical dispersion to be unimportant.

There are well established, although essentially quasi-empirical, continuum models that account for dynamics on the scale of the pores or for inertial effects: the Brinkman equation is the most common means of incorporating internal viscous deformation in the fluid as well as simple viscous drag on the porous matrix, while the Forchheimer equation is a non-linear extension of Darcy's law which parameterises quadratic inertial drag as well as linear viscous drag (see [20]). In the majority of this review, however, the two limits in (2.10)–(2.11) are assumed to hold. It should be noted that these limits are not physically unreasonable in geological contexts even for convection at very high Ra. For example, a very permeable sandstone ($k = O(10^{-11}\mathrm{m}^2)$) saturated with water, with a density difference $\Delta\rho = O(10\,\mathrm{kg/m}^3)$ (appropriate for, say, a 50° temperature difference or a full saturation of CO_2 in water) could have a buoyancy velocity as large as $\hat{u} = O(10^{-5})$ m/s (*i.e.* timescales on the order of days to travel 1 m). In a 100m-deep aquifer, we could have $Ra \sim 10^4$ or larger, while the ratios in (2.10)–(2.11) can both remain several orders of magnitude smaller than unity (*e.g.* for thermal convection in water with $\kappa \sim 10^{-7}$ m^2/s, $\hat{u}k^{1/2}\rho/\mu \sim 10^{-4}$ and $\hat{u}k^{1/2}/\kappa \sim 10^{-3}$). In less permeable rocks, these ratios would be even smaller.

(e) Solution approaches

Progress in solving the governing equations (2.1)–(2.5) numerically can be made by eliminating either the velocity or the pressure from Darcy's law. In the former case, the constraint of incompressibility leaves a Poisson equation for the pressure. However, in most situations one knows information about the velocity components at the boundaries, rather than the pressure, and so it is more convenient to eliminate pressure. In two dimensions, this is easily achieved by introducing the vorticity vector $\boldsymbol{\Omega} = (\Omega_x, \Omega_y, \Omega_z) = \boldsymbol{\nabla} \wedge \boldsymbol{u}$ as in (2.9), which satisfies

$$\Omega_x = \Omega_z = 0, \quad \Omega_y = -\frac{kg\rho_0\alpha_T}{\mu}\frac{\partial T}{\partial x} = -\nabla^2\psi, \tag{2.12}$$

(shown here for the case of thermal convection). The final equality in (2.12) follows after introduction of a streamfunction ψ for the flow, satisfying $\boldsymbol{u} = (u, w) = (\psi_z, -\psi_x)$, and gives an

	Some examples	Notes
Numerical simulations:		
Pseudo-spectral	TS: [35,36]; OS: [37]	Fast solvers.
Finite difference (+ spectral)	TS: [38,39]; OS: [40–42]	More flexible for applying different boundary conditions or using stretched coordinates.
Finite element	OS: [43,44]	Not widely used. More flexible again for dealing with internal boundaries and adaptive grid spacing.
Experiments:		
Hele–Shaw cell:	OS: Glycol mixtures; [41,45–47]	Non-monotonic equation of state; interface moves over time; some viscosity variation with concentration.
	OS: $KMnO_4$-water; [48,49]	Approximately linear equation of state; possible to maintain fixed interface.
	TS: Temperature; [50]	Easy to apply fixed boundary conditions; challenges associated with heat loss.
Porous medium:	OS: Glycol mixtures; [51,52]	As above.
	TS: Temperature; [50,53,54]	As above, with additional challenges of heat transfer in solid phase.

Table 1. A summary of different numerical and experimental approaches to modelling high-Ra two-sided (TS) and one-sided (OS) convection in porous media, together with some example citations to which the interested reader is referred for more details. Finite difference (+ spectral) indicates that horizontal Fourier Transforms might be used in conjunction with a finite-difference (typically second-order or compact fourth-order) discretization (e.g. to solve (2.12)). The relative merits of Hele–Shaw cells and idealised porous media (e.g. bead or fibre packings) are discussed in §2(f).

elliptic equation for the streamfunction, which can be solved in conjunction with the transport equation (2.5) (alternatively, the streamfunction can be avoided altogether by means of a further derivative of (2.12), which, together with the constraint of incompressibility, yields $\nabla^2 w \propto \partial^2 T/\partial x^2$). The vast majority of numerical studies of high-Ra convection have employed either pseudo-spectral or finite-difference techniques to solve these equations (see table 1).

In three dimensions, a more convenient method arises if one exploits the vanishing vertical vorticity and the divergence of the velocity to write the velocity field in terms of a scalar potential function, $\boldsymbol{u} = (u, v, w) = \nabla \wedge (\nabla \wedge \hat{\psi}\boldsymbol{e_z})$ [34]. Eliminating the pressure from (2.2) and integrating in z now yields

$$\nabla^2 \hat{\psi} = -\frac{kg\rho_0\alpha_T}{\mu} T, \tag{2.13}$$

which can again be solved in conjunction with the transport equation (2.5).

Finally, it is well known that one does not have the freedom to impose as many boundary conditions on porous-media flow as on unconfined flow, because of the absence of velocity derivatives in Darcy's law. As such, one can typically specify normal velocities but not tangential velocities on boundaries, as reflected in the fact that (2.12)–(2.13) are second-order equations for the streamfunction or potential, whereas the unconfined vorticity equation, written in this manner, would give fourth-order equations.

(f) Experimental approaches

To model convection in porous media in a laboratory experiment, there are two key considerations. The first is how to model the medium: generally one either uses idealised granular media such as packings of spherical beads, or a Hele–Shaw cell. The Hele–Shaw cell is a narrow slot which mimics two-dimensional flow in porous media; the thickness of the slot controls its 'permeability', and it has the great advantage of clear optical access, while lacking any of the complexity (and realism) of tortuous porous pathways, variable pore sizes and three-dimensional flow (assuming the slot remains sufficiently thin relative to the lengthscales of the flow). Packings of beads provide a convenient analogue medium, but optical access is generally limited. Inevitably, in either case it is difficult to replicate the range of scales found in many natural settings (a kilometre-scale sandstone aquifer could have pore sizes on the scale of microns, for example), while practical considerations of time and scale often render it sensible to use a larger

permeability in a laboratory experiment than in the natural setting, which can have implications for whether experiments violate some of the assumptions outlined in the previous section.

The second key consideration in experimental modelling of convection in porous media is how to drive the convective motion. While some experiments, particularly those focussed on the two-sided setup, have used temperature to drive convection, many studies have used solute, because issues associated with heat loss from the apparatus are nullified and the solutal diffusivity is often smaller than the thermal diffusivity, leading to higher values of Ra for the same density difference and tank size. Because of its relevance to the convective dissolution of CO_2, various studies have also employed miscible fluid mixtures that have a non-monotonic density profile as a means of generating one-sided convective flow, as discussed in §4(c). A summary of different experimental modelling approaches to high-Ra porous convection is given in table 1.

3. Two-sided convection

Perhaps the simplest and most canonical system in which to study convective flows is the Rayleigh–Bénard cell, in which the upper boundary is cooled and the lower boundary heated so that the dynamics within the cell evolve to a steady or statistically steady state. In a fluid-saturated porous medium, this convective system is typically named after some combination of Horton, Rogers, Lapwood, Rayleigh, Darcy, and Bénard; where we need to refer to it here, it will be labelled a 'Rayleigh–Darcy' cell. This system is studied not because it directly models most physical systems but because it allows for a clear and detailed examination of the buoyancy transport, dynamics and flow structures of convection. We will discuss this setup from a theoretical and computational perspective initially, before considering variations of the system that incorporate additional physics, and some experimental observations.

The typical setup for the Rayleigh–Darcy cell is shown in figure 1a: a cell of height H, in two or three dimensions with either periodic or insulating (no flux) conditions on the side walls and, on the upper and lower boundaries, a fixed temperature and no normal flow,

$$T(z=0)=\Delta T, \quad T(z=H)=0, \quad w(z=0,H)=0. \tag{3.1}$$

The height H of the cell, together with the driving density difference $\Delta\rho=\alpha_T\rho_0\Delta T$, buoyancy velocity $\hat{u}$ (2.6) and associated convective timescale $\hat{t}=\overline{\phi}H/\hat{u}$ can be used to render the governing equations in non-dimensional form. Scaling lengths with H, velocities with $\hat{u}$ and time with $\hat{t}$, one arrives at

$$\boldsymbol{\nabla}\cdot\boldsymbol{u}=0, \qquad \boldsymbol{u}=-\boldsymbol{\nabla}P-T\hat{\boldsymbol{z}}, \qquad \frac{\partial T}{\partial t}=\boldsymbol{u}\cdot\boldsymbol{\nabla}T=\frac{1}{Ra}\nabla^2T, \tag{3.2a, b, c}$$

where $P=(p+\rho_0gz)/(\rho_0\alpha_T\Delta TH)$ is a dimensionless effective pressure. The Rayleigh number Ra takes the form of an inverse diffusivity in the advection–diffusion equation (3.2c). [2]

A key quantity of interest is the degree to which the transport, or flux, of buoyancy is enhanced by convective motion. A dimensionless measure of this convective flux is given by the Nusselt number (or, for solutal systems, the Sherwood number), which provides the ratio of the total flux F^* of buoyancy to the diffusive flux that would occur if there were no convection,

$$Nu=\frac{F^*}{\kappa\,(\Delta\rho/H)}, \tag{3.3}$$

If there is no convection, $Nu=1$. One can calculate the Nusselt number by integrating the flux across any height z; in a steady state, the flux through any slice must be equal. Given the boundary conditions of no normal flow at the boundaries, it is often convenient to calculate the Nusselt

[2]Note that one could alternatively choose a diffusive scale for velocity and time, which would lead to the Rayleigh number multiplying the right-hand-side of (3.2b) instead; this approach is avoided here because it results in velocity scales and convective overturning timescales for the flow at high Ra that are $O(Ra)$, rather than $O(1)$.

number by integrating the total flux entering the system (by diffusion) at the boundaries to yield

$$Nu = -\left\langle \left.\overline{\frac{\partial T}{\partial z}}\right|_{z=0} \right\rangle, \tag{3.4}$$

where the over-bar and the angle brackets indicate a horizontal and a long-time average, respectively. In fact, it is relatively straightforward to manipulate (3.2c), together with the boundary conditions and the incompressibility constraint, to derive equivalent expressions for the Nusselt number in terms of integrals over the entire (dimensionless) domain,

$$Nu = 1 + Ra\left\langle \int_0^1 \overline{wT}\,\mathrm{d}z \right\rangle = \left\langle \int_0^1 \overline{|\boldsymbol{\nabla} T|^2}\,\mathrm{d}z \right\rangle, \tag{3.5}$$

(e.g. [38,55]). In fact, the first equality in (3.5) is often taken as the explicit definition of Nu, from which (3.4) can be derived. Note the importance of the long-time average: when the flow in the cell is unsteady, then the quantities inside the angle brackets in these expressions will not, in general, yield the same result at any particular time t. The final expression in (3.5) is a measure of the scalar (in this case, thermal) dissipation rate; this quantity is often used in studies of turbulent flows, and is an important measure of mixing in evolving flows in porous media (e.g. in viscous fingering [56] or evolving convection [40], as discussed briefly in §4 below).

(a) Overview of low-Ra dynamics

The Rayleigh number Ra is the main parameter that controls the dynamics in the Rayleigh–Darcy cell. (If the cell has a finite lateral extent, then its aspect ratio can also play an important role; for the purposes of this overview, the lateral extent of the cell is considered to be sufficiently large that the aspect ratio is unimportant.) Convection in a two-dimensional Rayleigh–Darcy cell for low and moderate values of Ra has been the subject of various studies (see [20]). It is straightforward to show by linear-stability analysis that for $Ra < Ra_{crit} = 4\pi^2$, a vertically linear and horizontally uniform temperature field is stable [57]; the dissipative effects of diffusion and viscosity are too large; there is no flow and the buoyancy transfer is purely diffusive ($Nu = 1$). For larger values of Ra the flow takes the form of large-scale convective rolls and Nu increases (figure 2a). These rolls are steady for sufficiently low Ra, but boundary-layer instabilities result in a series of bifurcations to the flow as Ra is increased which perturb, but do not completely destabilize, the background cellular structure [58–60]. For $Ra \gtrsim 1250$, however, the quasi-steady background rolls are completely broken down by the growth of destabilizing plumes from the upper and lower boundaries of the domain [38,39]. The reorganisation of the dynamical structure is reflected by a notable drop in the convective flux (the kink in figure 2a), and marks the transition to the 'high-Ra' regime of interest here. (There is not a precise value of Ra at which this regime starts; the dynamics exhibit significant hysteresis [38] and depend on the lateral extent of the domain). The three-dimensional cell has received rather less study, but similar qualitative behaviour is observed: the additional degree of freedom certainly leads to a richer range of dynamics and emergent patterns as Ra is increased [61], but again there is a transition at $Ra \approx 1750$ to a new dynamical regime.

(b) High-Ra convection

Flow in the high-Ra regime takes quite a different form from the unit-aspect-ratio roll-like structures that persist for lower Ra. Figure 3(a) shows a snapshot of the temperature field in a two-dimensional Rayleigh–Darcy cell at $Ra = 5 \times 10^4$. The flow is dominated throughout the interior of the cell by vertical exchange flow comprising interleaving columns of hot and cold fluid with a Ra-dependent horizontal wavelength. Heat is transported through the upper and lower boundaries by thin diffusive boundary layers, which are unstable to the growth of short-wavelength and intermittent plumes. Between the relatively ordered interior flow and the boundary layers is a region that is dominated by vigorous mixing and transient flushing of

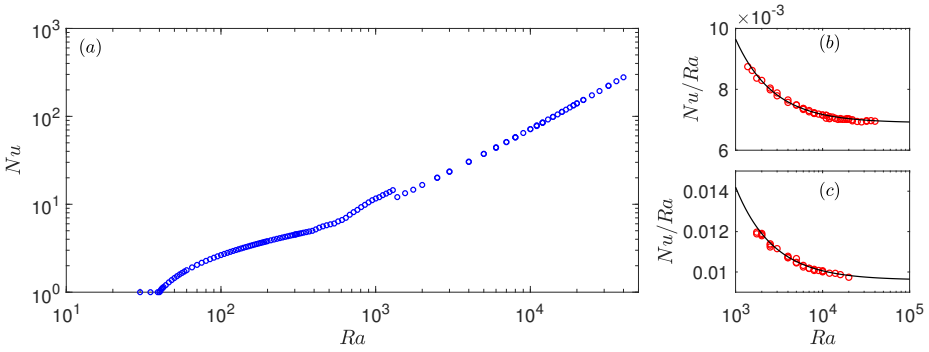

Figure 2. (a) The dimensionless flux Nu as a function of Ra from numerical simulations of two-dimensional 'two-sided' convection, taken from [39]. (b) The scaled Nu in the high-Ra regime, together with the fit (3.6) (solid line). (c) The scaled Nu in the high-Ra regime from equivalent three-dimensional simulations (taken from [61]), together with the fit referenced in the text (solid line).

these short-wavelength plumes, as heat is transferred between the boundary layers and interior exchange flow. Hewitt et al. [39] labelled the interior columnar flow and the short-wavelength plumes near the boundaries as 'megaplumes' and 'protoplumes', respectively. The horizontally averaged temperature (figure 3b) shows clearly the presence of the boundary layers at the upper and lower boundaries of the cell, and indicates that the mean temperature in the interior has a weak and roughly linear vertical gradient that decreases with increasing Ra.

In three-dimensions, a similar flow structure is observed (figure 4). The interior flow is again dominated by interleaving columnar exchange flow, while near the boundary the protoplumes take the form of thin filamentary sheet-like structures, which flush into the roots of the columnar flow. Again the interior appears to be relatively well ordered, compared with the more vigorous mixing and flushing near the boundaries.

(i) The convective flux

The instantaneous convective flux transported by the system at high Ra exhibits chaotic fluctuations about a mean, and a long-time average yields the Nusselt number Nu. In the usual Rayleigh–Bénard problem in an unconfined fluid, the relationship between Nu and Ra had proved an enduring subject of fundamental interest, and a number of theoretical predictions exist for the form of the relationship for large Ra (see, e.g. [19,21,22]). The presence of a Prandtl number in that system, and the relative sizes of the thermal and viscous boundary layers, provides significant complexity. The situation in a porous medium, where there is no no-slip condition and thus no viscous boundary layers near the upper and lower boundaries, is somewhat simpler.

Perhaps the simplest argument for the convective flux at high Ra is that of the 'marginally stable boundary layer' proposed for an unconfined fluid by Malkus and Howard [62,63]. This simple argument supposes that at sufficiently high Ra the interior flow mixes up fluid efficiently, confining the dominant vertical temperature gradients to narrow boundary layers at the upper and lower boundaries, with an $O(1)$ temperature contrast across them. The Nusselt number is thus just given by the diffusive heat flux across these layers, which is inversely proportional to their depth. The argument goes that the boundary-layer depth should be held at a marginal value, with any growth beyond that depth being rapidly scoured away into the interior flow. More precisely, the local Rayleigh number, defined in terms of the boundary-layer depth δ, is held at some marginal value Ra_{crit}. In an unconfined fluid, the Rayleigh number is proportional to the lengthscale cubed and this argument yields a prediction $\delta \sim 1/Ra^{1/3}$, ignoring factors of the constant Ra_{crit}, or $Nu \sim 1/\delta \sim Ra^{1/3}$. In a porous medium, the argument instead yields $\delta \sim 1/Ra$ or $Nu \sim Ra$. Note that if this linear asymptotic scaling holds, the dimensional buoyancy flux

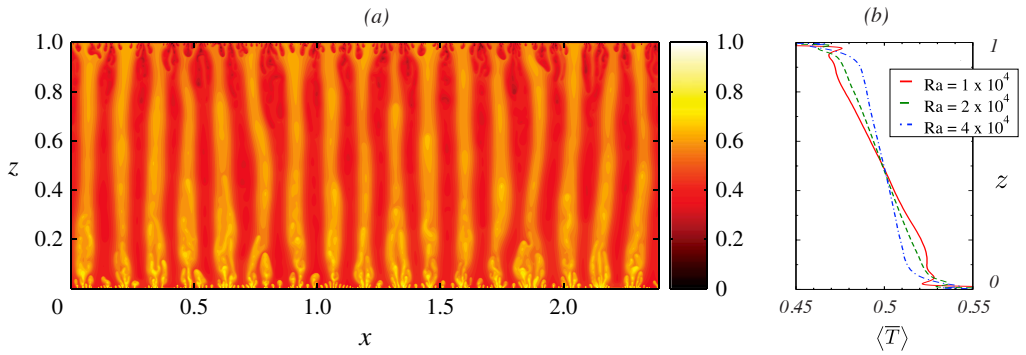

Figure 3. (a) Snapshot of the temperature field in a two-dimensional 'two-sided' cell for $Ra = 5 \times 10^4$, taken from [35]. (b) Time-averaged and horizontally averaged temperature as a function of depth for different values of Ra as marked, adapted from [39]. The temperature range in (b) is suppressed to show the weak linear slope in the interior; the majority of the vertical temperature drop takes place across the thin thermal boundary layers located at the upper and lower boundaries, which are too narrow to be seen on the scale in (a).

$F^* = \kappa \Delta\rho Nu/H$ is independent of both the depth H of the domain and the thermal diffusivity κ as $Ra \to \infty$. [3]

Beyond this simple scaling estimate of the asymptotic relationship $Nu \sim Ra$, various authors have tried to constrain the relationship by deriving rigorous upper bounds on $Nu(Ra)$. This is a problem of substantial mathematical richness and complexity, with links to more general problems in unconfined-fluid convection and turbulent flow; the interested reader is referred to the papers referenced here for more details. The earliest efforts to bound the flux for porous convection [67,68] built on techniques developed by Howard [69] using variational methods and energy equations to bound quantities in turbulent, statistically stationary flow. Subsequent studies [38,70] applied the so-called 'background' variational method to find asymptotic bounds consistent with the posited linear scaling, first of $Nu \leq (9/256)Ra$ [70] and then the tighter bound of $Nu \leq 00296Ra$ [38]. This background method, which, very crudely, is a variational approach in which the temperature field is decomposed into a steady background component and a time-dependent fluctuation field, where the background field satisfies a certain integral constraint, has subsequently been used to determine rigorous and non-trivial numerical improvements to these bounds [71,72], at least up to $Ra \approx 26500$. These improved bounds are also consistent with an asymptotic linear scaling.

The first well-resolved numerical computations of high-Ra convection in a two-dimensional Rayleigh–Darcy cell [38] extracted values of Nu up to $Ra = 10^4$ which suggested that the scaling exponent for the relationship $Nu(Ra)$ was slightly sub-linear, raising the question of whether the upper bound was attained in reality. However, subsequent computations [39] that extended up $Ra = 4 \times 10^4$ indicated that the linear scaling $Nu \sim Ra$ is attained asymptotically, but that there is a small constant correction to the linear scaling. This numerical data is well described by a simple fit,

$$Nu = \alpha Ra + \beta, \qquad \alpha \approx 6.9 \times 10^{-3}, \quad \beta \approx 2.75, \tag{3.6}$$

in the high-Ra regime ($Ra \gtrsim 1250$; see figure 2b). The dimensional buoyancy flux corresponding to (3.6) as $Ra \to \infty$ is $F^* = \alpha k g (\Delta\rho)^2/\mu$.

[3] Another classical argument for the unconfined Rayleigh–Bénard cell [64,65] yields a posited 'ultimate' regime $Nu \sim Ra^{1/2}$ as $Ra \to \infty$, although its existence continues to be a contentious subject (e.g. [66]). According to this argument, shear-driven turbulence in the boundary layers at extremely high Ra allows for an enhancement to the flux, which becomes asymptotically independent of the thermal diffusivity. Clearly such a mechanism is not possible in an inertia-free porous medium, although it is interesting to note that, unlike in an unconfined fluid, the requirement the flux be independent of the thermal diffusivity in a porous medium yields the same linear scaling $Nu \sim Ra$ as the Malkus–Howard marginal-boundary-layer argument.

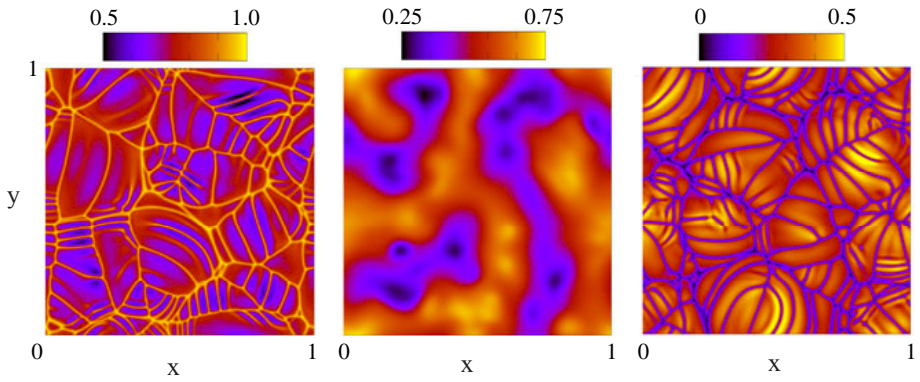

Figure 4. Slices of the temperature field in a three-dimensional 'two-sided' cell, at depths, from left to right, $z = 30/Ra$ (near the lower boundary), $z = 0.5$ (the midplane), and $z = 1 - 30/Ra$ (near the upper boundary), for $Ra = 8000$. Taken from [61].

The case in three dimensions appears to be much the same: equivalent direct numerical simulations in three dimensions [61] suggest a fit for $Nu(Ra)$ of the same form as (3.6) but roughly 40% higher, with $\alpha \approx 9.6 \times 10^{-3}$ and $\beta \approx 4.6$ (see figure 2c). Note that these simulations only extended up to $Ra = 2 \times 10^4$, and well resolved simulations at higher Ra would be needed to confirm this trend.

(ii) Structure of the flow

The interior columnar exchange flow in the cell is quite unlike the disordered turbulent dynamics encountered in pure fluid convection at high Ra. Hewitt et al. [39] found that, as Ra is increased, the interior flow away from the upper and lower boundaries becomes increasingly well described by a simple single-Fourier-mode steady solution of the governing equations, which they labelled a 'heat-exchanger' flow. This solution comprises an exact balance between vertical advection of a background temperature gradient and horizontal diffusion between columns, and takes the form

$$T - \frac{1}{2} = \hat{T} \sin(kx) - \frac{k^2}{Ra}\left(z - \frac{1}{2}\right), \quad w = \hat{T} \sin(kx), \quad \text{and} \quad u = 0, \tag{3.7}$$

where k is the horizontal wavenumber that increases with Ra, and the amplitude $\hat{T}$ tends to a constant as Ra is increased. The heat flux carried by this flow is $\hat{T}^2/2$, and so the fact that $\hat{T}$ tends to a constant is equivalent to the fact that the linear scaling of $Nu(Ra)$ is attained asymptotically.

While the interior flow is increasingly well described by this steady exchange flow solution as Ra is increased, the manner in which it matches to the complex dynamics near the upper and lower boundaries is not straightforward. Here, the flow remains strongly time-dependent, and, indeed, the dynamics of merging between protoplumes appears to get more complex as Ra is increased. In part the reason for this is that the horizontal scale of the short-wavelength protoplumes (or, in three-dimensions, the protoplume filiments) decreases more rapidly with Ra than the scale of the interior flow, meaning that there are increasingly many protoplumes between each megaplume root as Ra is increased. More specifically, the protoplume width decrease like Ra^{-1} [39,61], which is the intrinsic advection–diffusion lengthscale of the flow, but the horizontal scale of the interior flow has a much weaker dependence on Ra. Various studies in two-dimensions have confirmed that the interior horizontal wavenumber k increases with an exponent of the Rayeigh number slightly less than 0.5 (figure 5); computations by [39] give an empirical fit $k = 0.48Ra^{0.4}$, also included in figure 5. In fact, some more recent computations in two dimensions [73] yielded a different fit for k with an exponent much closer to 0.5, but these computed values are differ systematically from all the results shown in figure 5, suggesting that

perhaps mode restriction from the aspect ratio in these computations is disrupting the realised horizontal lengthscales of the megaplumes.

In three-dimensions there are insufficient results at high enough Ra to give a firm scaling for the mean horizontal wavenumber, but, unlike in two dimensions, the available computations are consistent with a scaling of $k \sim Ra^{0.5}$ [61].

The question of what controls the horizontal scale of the interior flow has motivated various studies [34,35,74], since it is evidently not controlled directly by the scale of the flow at the boundaries. One approach [35] has been to find exact steady solutions of the governing equations in a finite domain that have the same qualitative structure as the unsteady flow, with thin boundary layers at the boundaries and an interior columnar exchange flow. Wen et al. [35] explored the stability of this base state, and identified two dominant types of instability, characterized by 'bulk' or 'wall' modes, with the wall modes being strongly localized to the upper and lower boundaries. They argued that the nonlinear evolution towards fully developed statistically steady flow resulted, in general, from an interplay of these two modes: the wall modes drive apart wide columns by the growth of small protoplumes from the boundaries, while the bulk mode drives coarsening of overly narrow columns.

A different approach [34,74] has been to use information about the the stability of unbounded 'heat-exchanger' flow to generate a prediction as to whether the horizontal scale of the bounded flow in the cell is controlled by its stability. In two-dimensions, this approach suggests that the columnar flow would be unstable if the wavenumber had an asymptotic scaling greater than $k \sim Ra^{5/14}$ as $Ra \to \infty$, while in three dimensions the nature of the instability is somewhat different and the equivalent asymptotic prediction turns out to be $k \sim Ra^{1/2}$. According to this argument, the high-wavenumber dynamics of protoplumes at the boundaries continually force the interior flow at short scales ($\sim Ra^{-1}$), but the interior flow must coarsen until its wavenumber crosses the relevant stability bound ($k \sim Ra^{5/14}$ or $k \sim Ra^{1/2}$) [34]. These predictions are consistent with the available results from computations in two and three dimensions.

Well resolved numerical results at higher Ra, particularly in three dimensions, are needed to further address the the question of what controls the horizontal scale of the interior flow. However, it is worth highlighting a caveat pointed out by Wen et al. [35] who found that the flow can become so well ordered in two dimensions at high Ra that the interior structure can become 'locked' with different numbers of plumes, and can persist in such a state for a very long time. Multiple computations for the same value of Ra can thus give different numbers of plumes (see highest data in figure 5), indicating that a great deal of caution is required when averaging the wavenumber at very large Ra.

(c) Variations

A number of studies have considered extensions to this basic setup, to consider the effect on convection of additional physical complexity, like heterogeneity in the medium or flow-dependent dispersion. In most cases, these additional physics have been explored for low-Ra convection and these studies are comprehensively reviewed elsewhere [20]. The focus here is on the few studies at high Ra.

(i) Inclined convection

If a Rayleigh–Darcy cell is sloped at an angle ϕ to the horizontal, standard linear-stability analysis reveals that the steady base state in three dimensions is stable for $Ra\cos\phi < 4\pi^2$ [75,76]. However, some of these unstable modes are three-dimensional; the two-dimensional cell has a different stability boundary, becoming linearly stable for all Ra for $\phi > \phi_{crit} = 31.49$ [76,77], although sub-critical instabilities in the two-dimensional cell can still give rise to non-linear convection for any angle $\phi \leqslant 90^\circ$ [78].

The dynamics of the two-dimensional cell at high Ra were explored in detailed numerical and theoretical study by Wen and Chini [78]. They found that, as the inclination angle ϕ is increased

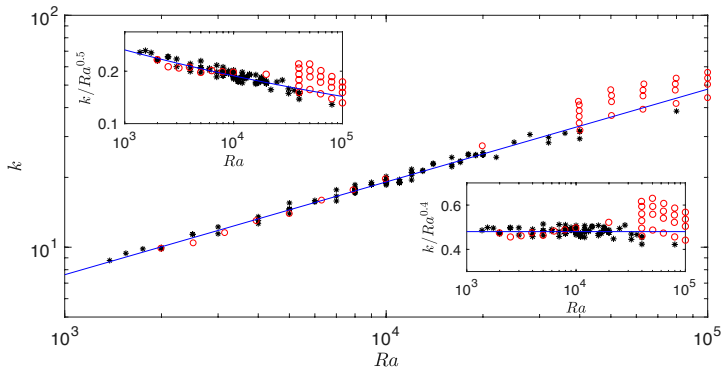

Figure 5. The dominant horizontal wavenumber of the interior flow for two-dimensional porous convection, taken from [39] (black stars) and [35] (red circles), together with the fit $k = 0.48Ra^{0.4}$ (blue line). The insets shows the same data scaled by $Ra^{0.5}$ and $Ra^{0.4}$ as marked.

the basic structure of the high-Ra flow in a horizontal layer, with wall-localised protoplumes and interior columnar flow, is preserved for $\phi \lesssim 25^\circ$, although the interior plume spacing increases as the columns are perturbed by the tilting of the cell. The convective flux Nu decreases only weakly over this range of angles; indeed, it can increase slightly above the value in a horizontal layer for small angles, which presumably reflects that a slight perturbation to the interior columnar structure can lead to a flow pattern that, from the point of view of maximising the buoyancy transport, is slightly more optimised. However, above a critical angle that is remarkably close to the critical angle ϕ_{crit} for linear stability in two dimensions (around 30°), the columnar structure of the flow is completely broken down: there is a transition to a large-scale travelling-wave convective roll state and the convective flux is substantially reduced from its value in a horizontal layer.

(ii) Layered convection

The effect on vigorous convection in a Rayleigh–Darcy cell of horizontal layering in the medium was explored by Hewitt et al. [79]. They focussed on the impact of a thin, low-permeability horizontal layer located at the centre of the cell in two dimensions; such layers are common features in natural sedimentary formations. In the limit that both the thickness h and permeability k of the low-permeability layer are small relative to the depth H of the cell and permeability K of the host medium, the flow can be described solely by a measure of the layer's impedance $\Omega = (h/H)/(k/K)$ and by Ra (as had been shown previously for low Ra convection [80]). This study found two notable features as the impedance Ω of the layer is increased. First, the interior columnar plumes in the cell are driven further apart (see e.g. figure 6a), with their dominant horizontal scale increasing roughly like $\Omega^{1/2}$, and second the buoyancy flux Nu decreases (although, remarkably, for small Ω it can in fact increase slightly above its value in the homogeneous cell, which, as for the case of inclined convection, is presumably related to the change in interior structure induced by the layer). Above a critical value of $\Omega \approx 5$, the impedance of the layer becomes so large that diffusion, rather than advection, becomes the dominant mechanism of buoyancy transport across it. For higher values of the impedance, the cell simply resembles two stacked Rayleigh–Darcy cells placed one above the other, with a diffusive boundary between them.

(iii) Anisotropic convection

The case of an anisotropic permeability field - that is, a different permeability in the horizontal and vertical directions - was considered in a numerical study by De Paoli et al. [73], motivated by the

fact that sedimentary formations often have less resistance to flow in the horizontal plane than in the vertical. They explored the impact of the ratio of vertical to horizontal permeability $k_v/k_h \leqslant 1$ on statistically steady high-Ra convection; specifically, they fixed the vertical permeability in order to scale the problem, and then found that the convective flux increases as k_h is increased (roughly like $k_h^{0.25}$) while the interior wavenumber also increases (roughly like $k_h^{0.4}$; that is, the plumes become narrower). Presumably the increased flux arises because a reduction in the horizontal resistance enhances the horizontal flushing near the boundaries into interior megaplumes, and thus increase the vertical advective transport carried by the interior flow.

(iv) Dispersion

A number of experimental studies of convection in porous bead packs (*e.g.* [52,81,82]) have demonstrated that velocity-dependent mechanical dispersion can have a substantial effect on flow if the pore-scale Peclet number is substantially larger than unity. These studies suggest that both the buoyancy flux and the structures of convective flow can be significantly altered by this additional mixing mechanism; in particular, the relationship $Nu(Ra)$ can have an exponent that is distinctly sub-linear. In the context of statistically steady high-Ra convection, Wen et al. [83] presented a systematic numerical study of the effect of both longitudinal (in the flow direction) and transverse dispersion on the flow, and introduced the terminology of a *dispersive* Rayleigh number[4] $R_d = \hat{u}H/(\alpha_d \hat{u}) = H/\alpha$, where α_d is the transverse 'dispersivity', which is expected to scale with the pore size δ_p. In this terminology the ratio $Ra/R_d \sim \hat{u}\alpha_d/D$ can be thought of as the same pore-scale Peclet number introduced in §2(d)ii above: when $Ra/R_d \ll 1$ the dynamics are unaffected by mechanical dispersion, while for $Ra/R_d \gtrsim 50$ it is the dispersive Rayleigh number that controls the dynamics and the size of the flow structures and boundary layers [83]. The Nusselt number appears to retain a linear scaling with Ra, but with a prefactor that depends on R_d, which means that the actual dependence of the dimensionless flux on medium properties like the permeability - which also affects the dispersivity - can be more complex. Wen et al. [83] also explore the effect of anisotropy between longitudinal and transverse dispersion; in particular they show that the columnar structures of convection can be substantially disrupted by anisotropic dispersion, becoming somewhat wider and more 'fan'-shaped as the longitudinal dispersion becomes dominant (see e.g. figure 6b).

(d) Experiments, and the break-down of the porous-media construction

As well as the importance of dispersion, laboratory experiments have also shown how easy it is to violate the assumption implicit in Darcy's law that there is a separation of scales between the pore size and the characteristic lengthscales of the flow. The earliest experiments of this system [50,53] were thermally driven and undertaken in both three-dimensional bead or fibre packings and in quasi-two dimensional Hele-Shaw cells. These experiments found generally good agreement at low Ra with model predictions, but, although they show data consistent with the expected linear scaling $Nu \sim Ra$ for moderate Ra, they find the heat flux drops below this scaling for sufficiently large Ra. Elder [50] attributes this change in scaling to the fact that the thermal boundary layers are smaller than the pore scale, and so the flow is undergoing a transition to something more like unconfined viscous Stokes-flow convection. It should be mentioned that these impressive early experiments also produced some beautiful observations of columnar pattern formation: Elder [50] observed two-dimensional columns in a paraffin-filled Hele–Shaw cell akin to those in figure 3, while Lister [53] observed three-dimensional plume roots akin to those in figure 4, albeit at lower Ra (see e.g. figure 6c).

More recent experimental studies in bead packs [54,84] have similarly found that the structures of convection are smaller than the scale of the beads, and so the system is no longer really a porous medium, in a continuum sense. Indeed, in some of these experiments the pores are so

[4]Note that, assuming the dispersivity scales with the pore size, the dispersive Rayleigh number defined here is effectively a ratio of the macroscopic lengthscale H to the pore scale δ_p, and so $Ra_d \sim Da^{-1/2}$, where $Da = k/H^2$ is the Darcy number. The condition $Ra/R_d \ll 1$ simply reproduces the constraint in (2.11), $RaDa^{1/2} \ll 1$.

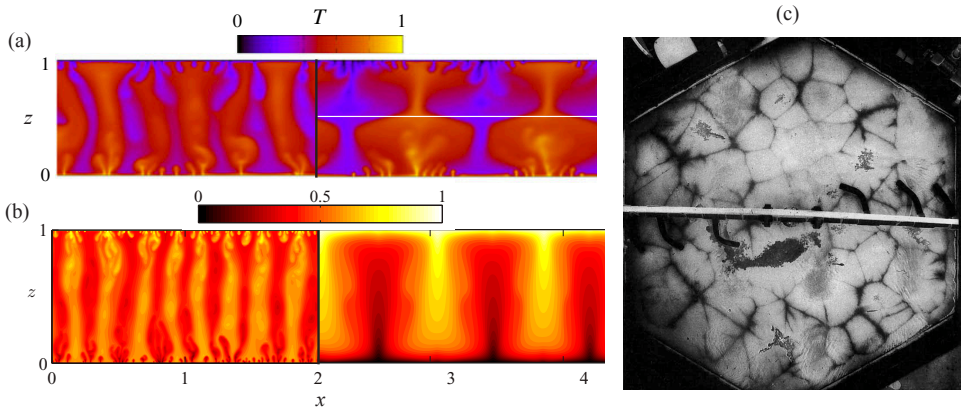

Figure 6. (a) A snapshot of the temperature field in cell containing a thin, low-permeability layer at its centre ($Ra = 5000$, $\Omega = 0$ (left) and $\Omega = 0.5$ (right), adapted from [79]. (b) A snapshot of the temperature field with anisotropic mechanical dispersion ($Ra = 20000$, $Ra/Ra_d \ll 1$ (left) and $Ra/Ra_d = 200$ (right), adapted from [83]. (c) A snapshot of the upper surface of one of Lister's experiments of porous convection, with dark regions showing dense downwelling plume roots ($Ra = 736$, taken from [53]).

large compared to the thermal boundary layers and flow structures that individual beads form macroscopic obstructions to the flow and, as suggested by Elder [50], the measured heat flux in the cell appears to approach that predicted for convection in a pure-fluid layer.

Note that this breakdown of Darcy's law is much more likely to be a problem at the analogue laboratory scale than in natural - certainly in geophysical - settings, as discussed in §2(d)iii, because of artificially large pore sizes relative to the other parameters of the problem. Nevertheless, this is evidently a limit that can be attained, and it presents some complexities for modelling. As noted in §2(d) above, there are various popular phenomenological or quasi-empirical continuum models which one can analyse, and numerous studies have done this in the context of low-Ra convection (see [20] for an overview). To my knowledge, these models have not been systematically investigated in the context of high-Ra convection. However, Letelier et al. [55] recently addressed this problem numerically by explicitly modelling flow in a Hele–Shaw cell but retaining the next-order corrections in powers of the slot thickness: they show that the flux decreases from the linear scaling in (3.6) as the slot width is increased, as internal fluid dissipation (rather than simply drag on the side walls) and inertial terms begin to play a role in the dynamics. While this approach does not model a porous medium directly, it provides a promising avenue to understand how solutions change when the dynamics become comparable to the microscopic lengthscale of the geometry.

An alternative route to understanding the limit in which Darcy's law begins to break down may be to move away from the continuum limit. Some studies have explored the break-down of Darcy's law for low and moderate Ra convection using the Lattice-Boltzmann method to describe flow between the pores of the medium (e.g. [85]), while Gasow et al. [86] recently presented direct numerical simulations of high-Ra two-sided convection that resolved flow on the pore scale through an idealised network. They found that resolving flow on the pore scale can lead to a reduction in the convective flux, and also demonstrated that the pore-scale dynamics can affect both the small (proto-plume and boundary-layer) scales and the large (megaplume) scales of the macroscopic flow.

4. Evolving, one-sided convection

Most natural settings in which convection arises would be better described by a source of buoyancy on one boundary than on two. Such 'one-sided' convection differs fundamentally from

the 'two-sided' situation described above because it evolves over time: the focus for the modeller is to understand and describe the transient behaviour, rather than the statistically steady state. Owing to its more direct applicability to physical situations - most particularly to the convective dissolution of CO_2 - this setup has received a great deal of attention over the last few years. While one could envisage convection above a heated plate, most authors have considered solutal convection driven by a distributed dense source along an upper boundary, again in light of its relevance to the CO_2-sequestration problem. We mirror that setup here, and consider the simplest case of a dense source along an upper impermeable boundary with an impermeable lower boundary at some distance far below the source (figure 1b). For the purposes of clarity, the main discussion here describes convection in an isotropic, homogeneous two-dimensional medium, and is based on the results of numerical simulations and theory. Some experimental results are then outlined, as are various extensions to account for additional physics.

Unlike for the two-sided situation considered above, where different Rayleigh numbers determine the different regimes of convection, the different regimes of flow associated with convection below one boundary occur as the flow evolves over time [37]. Initially, solute diffuses into the domain and a dense boundary layer will develop below the upper boundary. This will, in general, become unstable to convective motion after some time, leading to the development of short-wavelength plumes along the boundary layer (see, *e.g.*, figure 7). These transport solute efficiently away from the upper boundary, and, as they move and grow, they merge and coarsen in a complex, non-linear fashion. Over time, the flow is organised into a series of large, dense plumes which stretch far below the source, fed by vigorous mixing and flushing of smaller plumes at their roots near the upper boundary. At some point, these downwelling plumes reach the lower boundary of the domain, which causes solute to 'back-up' and results in a gradual reduction of the strength of convection as the entire domain becomes more and more saturated with dense fluid. Ultimately, convective motion in this closed domain will be 'shut-down' as the density difference between the upper boundary and the interior fluid weakens.

Suppose that a domain initially contains a fluid with zero concentration C of solute, and has an impermeable upper boundary, at which the solute concentration is held at ΔC, located at $z=0$ and a lower boundary at $z=-L$ (figure 1b). Given the unimportance of the lower boundary of the domain until the latter stages of the 'life-cycle' described above, it makes sense to use the intrinsic lengthscale $\tilde{H}$ over which advection and diffusion balance, $\tilde{H}=\phi D/\hat{u}$, as the natural lengthscale for this problem, written in terms of the buoyancy velocity $\hat{u}=\rho_0\alpha_C\Delta C g k/\mu$ (2.6). This is in contrast to the two-sided case discussed in the previous section, where the macroscopic depth of the domain was used as the length scale for non-dimensionalisation. Scaling lengths with $\tilde{H}$, velocities with $\hat{u}$, times with the associated advection–diffusion timescale $\tilde{t}=\phi\tilde{H}/\hat{u}=\phi^2 D/\hat{u}^2$ and concentrations with ΔC one arrives at

$$\boldsymbol{\nabla}\cdot\boldsymbol{u}=0, \qquad \boldsymbol{u}=-\boldsymbol{\nabla}P+C\hat{\boldsymbol{z}}, \qquad \frac{\partial C}{\partial t}+\boldsymbol{u}\cdot\boldsymbol{\nabla}C=\nabla^2 C, \tag{4.1a, b, c}$$

in place of (3.2), where the effective pressure is $P=(p+\rho_0 g z)/(\rho_0\alpha_C\Delta C\tilde{H})$. This choice of scaling leaves a parameter-free set of equations, and the Rayleigh number only appears as the dimensionless location of the lower boundary

$$z=-Ra=-\frac{L}{\tilde{H}}=-\frac{\hat{u}L}{\phi D}. \tag{4.2}$$

This scaling makes explicit the fact that the dynamics associated with the onset and early evolution of convection, assuming it is far from the lower boundary, cannot have any appreciable dependence on the Rayleigh number. With this choice of scaling the dimensionless advection–diffusion lengthscale (e.g. the scale one might expect for boundary layers and associated small plumes) is $O(1)$, rather than $O(1/Ra)$ as it is for the previous choice of scalings in §3.

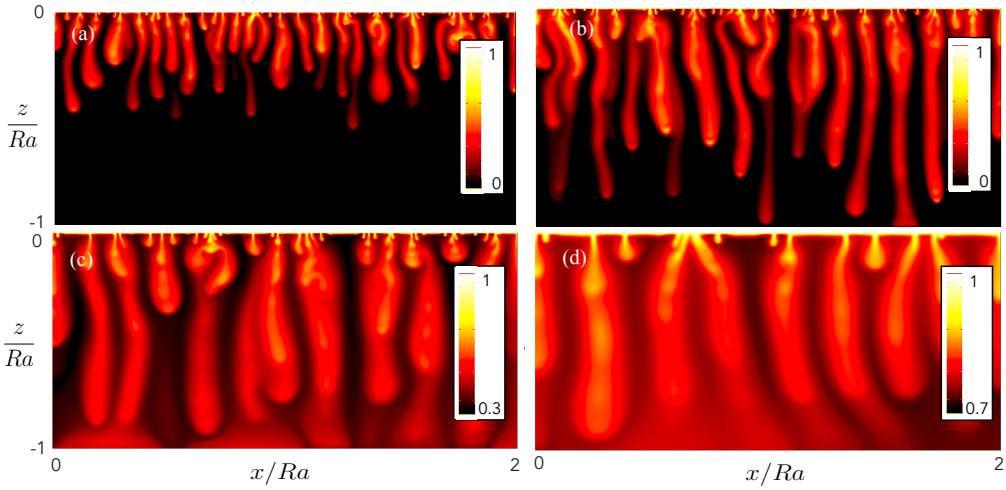

Figure 7. Snapshots of the concentration field from two-dimensional numerical simulations for $Ra = 10^4$ at times (a) $t = 4Ra$, (b) $t = 8Ra$, roughly when the plumes first hit the base, (c) $t = 32Ra$ and (d) $t = 128Ra$. Note the changing colour scale as the domain fills up with solute. Adapted from [41].

One is typically interested in both the evolution of the convective dynamics and in the dimensionless buoyancy flux F through the upper boundary,

$$F(t) = \overline{\left.\frac{\partial C}{\partial z}\right|_{z=0}}, \tag{4.3}$$

which, from the average of (4.1c), satisfies

$$\frac{\partial}{\partial t}\langle C\rangle = F, \tag{4.4}$$

where again the over-bar denote the horizontal average (*i.e.* over x and y) and now the angle brackets indicate the total volume integral $\langle C\rangle = \int_{-Ra}^{0} \overline{C}\,\mathrm{d}z$. The corresponding dimensional flux F^* of buoyancy is $F^*(t) = kg(\Delta\rho)^2 F(t)/\mu$.

Note that one could consider a more general measure of mixing, by analogy with studies of turbulent mixing (e.g. [87]) or other mixing problems in porous media (e.g. [56]), by tracking the scalar dissipation rate $\left\langle |\boldsymbol{\nabla} C|^2 \right\rangle$, which affects the second moment of the concentration via

$$\frac{\partial}{\partial t}\left\langle C^2 \right\rangle = 2\left(F - \left\langle |\boldsymbol{\nabla} C|^2 \right\rangle\right), \tag{4.5}$$

(this equation follows by multiplying (4.1c) by C and averaging). Note the difference from the statistically steady two-sided cell discussed in §3, where the Nusselt number (i.e. the flux) is equal to the dissipation rate (3.5). In this evolving system, by contrast, the dissipation rate and the flux combine to determine the evolution of the concentration variance $\left\langle C^2 \right\rangle - \langle C\rangle^2$ in the system, which is a measure of the degree of mixing, as explored by Hidalgo et al. [40]. Various studies have also used these ideas to propose methods of upscaling the problem of one-sided convection [37, 88]. In this review we will focus only on the flux F, which quantifies the total transport of solute into the domain without providing information on the mixing associated with that transport.

(a) Onset of convection

Initially, solute spreads below the dense upper boundary by diffusion. Assuming the lower boundary is far below ($Ra \gg 1$), the concentration in the initially growing layer has a

similarity solution $C \approx C_0(z,t) = 1 - \mathrm{erf}\,(\zeta/2)$, in terms of the similarity variable $\zeta = z/\sqrt{t}$. It is straightforward to generalise this expression to a finite domain if Ra is not large: the solution is no longer a function of one similarity variable but retains an explicit dependence on both time and space; see *e.g.* [89,90]. In the absence of gravity, this solution would remain stable and concentration would gradually diffuse through the entire domain. With gravity, however, the spreading layer becomes unstable to small perturbations and convective flow ensues, enhancing the transport of solute into the domain and raising the buoyancy flux across the boundary. The study of the instability process - how an evolving diffusive layer becomes unstable - has received an enormous amount of attention (*e.g.* [89–99]). While this is in part because questions of whether, and when, and in what manner, a diffusive layer becomes unstable are important for understanding how the system evolves, it also reflects the mathematical interest of a stability problem in which the base state changes in time. Since the onset problem is not the primary focus of this review, only a brief overview is provided here.

Perhaps the most straightforward approach to assess the stability of the evolving diffusive base state $C_0(z,t)$ is to employ a so-called 'quasi-steady-state approximation', in which one makes the assumption that any perturbations to the base state evolve on a much faster time scale than the base state itself, and so the time-dependence in in the base state can be 'frozen' (e.g. [89]). The advantage of this approach is that, having made the assumption, one can carry out a standard normal-mode linear-stability analysis. An obvious issue arises, however, when considering modes close to the onset of instability: one is often concerned with finding the time at which a particular mode becomes unstable, for example, which is precisely the point at which the approximation is worst, since the growth rate of the mode passes through zero. At large Ra, one can work in similarity, rather than physical, variables, which alleviates this issue because the base state is steady in similarity space. It does, however, raise other issues related to the space from which the perturbation modes can be selected (see e.g. [95]).

A more general, and more powerful, approach is that of non-modal, or 'generalised', stability theory [90,94,96]: very broadly speaking, the issue with the time-dependent linear perturbation equations here is that they give rise to a non-normal initial-value matrix equation, which means that the growth rate cannot be simply calculated from the eigenvalues of the perturbation matrix, as in a standard normal-mode analysis. Instead, one must effectively track an implicitly defined norm of arbitrary perturbations over time, allowing for the extraction of a measure of the instantaneous amplification or growth rate (e.g. [94]). Another alternative approach to the problem is simply to treat the linear perturbation equations as an initial-value problem for specific initial modes, which can be integrated forward to determine how they grows over time (according to some suitably defined norm, the choice of which can significantly affect the conclusions; see *e.g.* discussions in [97,99]). Or, in a different approach again, one can bypass the linear-stability problem altogether by considering the energy stability of the diffusive state (e.g. [90,91,93]).

Glossing over the details of these various different approaches, perhaps their key physical insights for understanding the evolution of the convective system at high Ra are that unstable modes will start to grow after dimensionless onset times $t \sim O(10^2)$, non-linear perturbations will be visible in the boundary layer after $t \sim O(10^3)$, and the associated lateral scale of these fingers will have a dimensionless wavelengths of the order of 100 (recall that lengths and time are non-dimensionalised by the intrinsic advection–diffusion scales $\tilde{H} = \phi D\mu/\Delta\rho g k$ and $\tilde{t} = D(\phi\mu/\Delta\rho g k)^2$, respectively). There are a wealth of studies that extend this stability problem to assess the role of additional physics, such as concentration-dependent viscosity [100,101], non-monotonic base density profiles [102], or the role of mechanical dispersion [103], anisotropy [89,93,104], heterogeneity [105,106] or chemical reactions [107,108].

As a cautionary note, it is perhaps important to balance the undoubted mathematical interest of this onset problem with the fact that in many physical systems in which $Ra \gg 1$, which are the focus of this review, the onset of convection will play only a small part in the overall evolution of the system; in such cases, understanding the longer-time evolution and shutdown described below may well be more important. It is also worth recalling that, in practical situations the initial

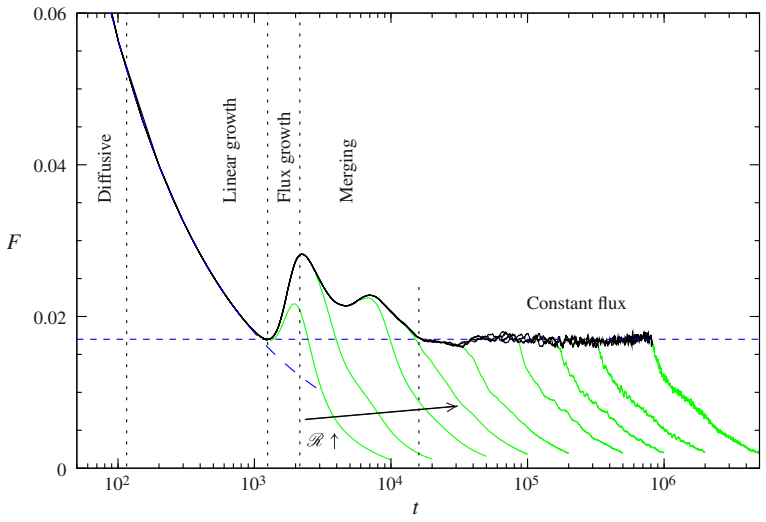

Figure 8. The buoyancy flux F through the upper boundary from simulations in a two-dimensional medium for a series of different values of Ra between $Ra = 100$ and $Ra = 5 \times 10^4$, taken from Slim [37]. The behaviour of the flux changes as the flow evolves through the different dynamical regimes marked. The only effect of the lower boundary - that is, Ra - is to determine the time at which the flow enters the final, 'shutdown' regime.

conditions are unlikely to be as simple as are often considered: during CO_2 sequestration, for example, the action of injecting the fluid into the rock and the subsequent lateral spread of the fluid under its own buoyancy may dominate the onset of convection.

(b) Evolution and shutdown

(i) Two dimensions

The overall evolution of the system from the onset of instability to the eventual shutdown of convection by saturation of the entire domain has been studied comprehensively in a two-dimensional medium by Slim [37], who identifies a number of dynamical regimes through which the system evolves. Figure 8, taken from [37], shows the evolution of the buoyancy flux through the upper boundary, which displays a clear signature of these different regimes. The initial diffusive solution has a flux that decays over time, and the first appreciable deviation from the pure diffusive solution in either the dynamics or in the flux arrives as non-linear interactions take hold of the instability: the growth of plumes in the boundary layer causes a slight reduction in its depth and a corresponding increase in the flux (the 'flux growth' regime in figure 8). This effect is inhibited as the plumes begin to interact and merge (the 'merging' regime in figure 8).

Once the plumes have coarsened sufficiently (after a dimensionless time $t = O(10^4)$; the precise time depends somewhat on the nature of the initial perturbations), a new dynamical regime is reached in which the flow takes the form of a series of larger plumes that are fed by small protoplume instabilities in the boundary layer at their roots (see e.g. figure 7a,b). This regime persists until the plumes feel the effect of the lower boundary of the domain. The flux in this regime displays chaotic oscillations about a constant value (figure 8) of $F \approx 0.017$ [37,109], which is perhaps surprising given that the domain is steadily filling up with solute. Slim [37] found that the descending plume tips fall at a roughly constant speed of $W \approx 0.13$, and behind them the horizontally averaged concentration $\overline{C}$ stretches in a rough wedge shape as a function of z/t,

$$\overline{C} \approx 0.27\,[1 + z/(Wt)] \quad \text{for} \quad z > -Wt, \tag{4.6}$$

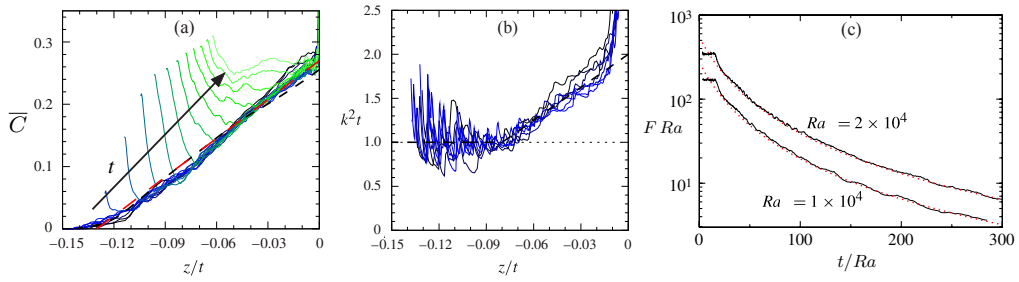

Figure 9. (a) The horizontally averaged concentration $\overline{C}$ and (b) the scaled dominant horizontal wavenumber k of the concentration field as a function of the similarity variable z/t for different times in the 'constant-flux' regime. (c) The (scaled) flux in the 'shutdown' regime for two different values of Ra as marked, together with the model predictions (red dotted). (a) and (b) are adapted from [37]; (c) is taken from [41].

deviating from this behaviour only when the plumes hit the base of the domain (figure 9a). The large descending plumes also coarsen over time with their average horizontal wavenumber decreasing like $t^{1/2}$. While a simple explanation of this scaling arises from a balance between advection in the interleaving plumes along the stretching base profile $W\partial\overline{C}/\partial z \sim t^{-1}$ and lateral diffusion between the plumes $\sim x^{-2}$, the true picture is more complex: the coarsening of the plumes is driven by the merging of plume roots in the boundary layer, which then propagates down the plumes at the roughly constant speed of the flow, to yield another self-similar profile as a function of z/t (figure 9b).

Once the first plumes have reached the base of the domain and this information has propagated back up to the upper boundary (at $t \approx 2Ra/W \approx 15Ra$ [37,41])), the supply of unsaturated fluid is used up and convection begins to 'shutdown'. An extensive study of this regime [41] has shown that the horizontally averaged concentration 'fills in' the wedge shape of (4.6) and become approximately independent of depth outside the upper boundary layer. The flow in this regime evolves in an almost quasi-statistically-steady manner as if it were the upper half of the 'two-sided' flow described in §3 above: the almost constant interior concentration gradually increases over time; the flux decreases and the convective dynamics weaken. Indeed, this analogy can be used to quantitatively predict the behaviour in this regime using the $Nu(Ra)$ flux law in (3.6). If we label the roughly constant interior concentration $C_i(t) = \int_{-Ra}^{0} \overline{C}(z,t)\mathrm{d}z$, then the driving concentration difference between the upper boundary and the interior is $1 - C_i(t)$. By considering the domain as the upper half of a 'two-sided' cell with total concentration difference $2(1 - C_i)$ and depth $2Ra$, and recalling the dependence of Nu and Ra on the height and concentration scales, one can rescale the relationship (3.6) to give an expression for the evolving flux $F(t)$ through the upper boundary in terms of the interior concentration $C_i(t)$,

$$F = Nu\frac{(1-C_i)}{Ra} = \frac{(1-C_i)}{Ra}\left[4\alpha\,(1-C_i)\,Ra + \beta\right] = 4\alpha\,(1-C_i)^2 + \frac{\beta\,(1-C_i)}{Ra}, \qquad (4.7)$$

where α and β were defined in (3.6). Integrating the advection–diffusion equation over the whole domain yields $dC_i/dt = F$, which can be integrated using (4.7) to give $C_i(t)$, and thus $F(t)$. In the limit of large Ra, this calculation shows that the interior concentration increases according to

$$C_i \approx 1 - \frac{1}{1+4\alpha t}, \qquad (4.8)$$

where $\alpha = 6.9 \times 10^{-3}$ as in (3.6). Predictions of the flux from this simple model give excellent agreement with the results of direct numerical simulations (figure 9c). The analogy with the two-sided cell also carries over into the evolution of the dynamical structures of convection [41]: the evolution of the dominant horizontal wavenumber can be quantitatively predicted from the equivalent wavenumber in the two-sided cell.

(ii) Three dimensions

The situation in three dimensions has not been explored in as much detail. Nevertheless, computations [42,44,109] suggest that the system evolves through the same dynamical regimes. Perhaps unsurprisingly, a rich variety of patterns emerge and develop as convection evolves in three dimensions [42]: these bare a qualitative resemblance to the structures observed in the two-sided cell (figure 4), although they evolve and coarsen over time. As in the two-sided system, these studies show that the convective flux is larger (by perhaps a factor of $20\% - 25\%$) than in two dimensions [42,44,109], but further studies would be required to more accurately constrain this observation.

(c) Experimental studies

A number of authors have undertaken laboratory experiments using analogue fluids to explore the behaviour of these one-sided systems experimentally. Most experiments of this system have used the narrow Hele–Shaw geometry as an analogue two-dimensional porous medium. Slim et al. [48] carried out experiments in a water-filled Hele–Shaw cell, with potassium permanganate crystals providing a dense source at the upper boundary. These experiments showed broad qualitative agreement with the theoretical description outlined above, from onset through to merging and interaction of the dense fingers, and ultimately to the shutdown of convection. This late-time behaviour was also studied experimentally in a Hele–Shaw cell in a different study [41] which, following earlier work [45], used a mixture of water and propylene glycol to drive convection. These miscible fluids have a non-monotonic density curve, and so a setup of one fluid above the other is initially stable but becomes unstable to convection as the fluids mix at the 'interface' between them. The modelling framework outlined above has also been extended to account for a retreating interface between two fluids [41], and such a system shows broad agreement of the late-time shutdown behaviour between model and experiment.

Notwithstanding these areas of agreement, there is one key difference between most experiments of the one-sided system and the theoretical and numerical results outlined above. Experimental measurements in the freely convecting 'constant-flux' regime consistently show that, although the convective flux is indeed roughly constant in time in this regime, it displays a weak but systematic variation with Ra (in terms of the scalings used in this review, it decreases with an exponent of Ra that varies between different studies but lies roughly between -0.3 and -0.1). These observations appear to be fundamentally at odds with the theoretical prediction of the idealised model (where, as shown explicitly by the scalings used here, Ra only enters the problem in the location of the base of the domain, and so cannot, plausibly, affect the flux in this regime), and have motivated a great deal of discussion. Backhaus et al. [45] and Ecke and Backhaus [46] observed such a decrease in detailed experiments using Hele–Shaw cells with water and propylene glycol to drive convection, while Tsai et al. [110] found a similar weak decrease in the flux with Ra in experiments in sloping Hele-Shaw cells. Similar results have also been obtained in various experiments with packings of glass or resins beads rather than Hele–Shaw cells [51,52,81,82], also using miscible glycol mixtures to drive convection.

While a conclusive explanation for this decrease in the flux remains elusive, there is a growing consensus that the relative size of the pore scale (or, in a Hele–Shaw cell, the gap width) to the lengthscales of the flow may lie at the root of the discrepancy (this ratio was highlighted in (2.11) above). Various studies have noted the potential importance of mechanical dispersion if the microscale is too large [52,82]. Liang et al. [52], for example, presented evidence that dispersion, rather than the driving buoyancy forces, becomes the primary control on the convective dynamics if the Rayleigh number Ra is much larger than the 'dispersive Rayleigh number', as discussed for the two-sided cell above in §3(c)iv). In that limit, dispersion leads to broader convective finger structures (as has also been observed in numerical simulations [111]), and there is a suggestion that the inherent anisotropy of mechanical dispersion may provide an explanation for observations of the decrease in the convective flux with increased Ra [52]. Very recently, De Paoli

et al. [49] carried out an impressive set of experiments using a similar setup to [48] (potassium permanganate in a Hele–Shaw cell) but at somewhat higher values of Ra, and demonstrated that the flux is, in fact, constant (that is, independent of Ra) if the gap width is sufficiently narrow, such that the lengthscales of the flow are all much larger than the gap width. Their study suggests that the widely observed decrease in the flux can be explained by non-ideal effects that arise when the gap width (or pore scale) becomes comparable to the intrinsic advection–diffusion lengthscales of the convective motion [5] , in agreement with the predictions of numerical simulations of the two-sided problem in a Hele–Shaw cell [55]. Indeed, this result is likely also to apply to the various bead-pack experiments that have been performed: back-of-the envelope calculations suggests that the advection–diffusion scale may indeed be somewhat smaller than the pore-scale in some of these experiments at large Ra, which would render Darcy's law inaccurate at the smallest scales.

Of course, there are other complexities to be considered when interpreting these various laboratory experiments. For example, some experiments feature an interface that recedes over time and is free to locally deform away from the horizontal, which can substantially enhance the flux [41]. In most analogue fluid mixtures, viscosity, as well as density, varies with the concentration, while the equation of state is typically non-linear. However, while the effects of these last two additional complexities on the evolution of one-sided convection have not been fully explored, numerical simulations in which these effects were considered [40] suggest that they are unlikely to be the primary explanation of the changing flux with Ra.

(d) Variations

A number of studies have gone beyond the relatively simple setup described above to investigate the effect of additional physics on the dynamics and buoyancy transport of one-sided convection in porous media.

(i) Heterogeneity and anisotropy

The role of an anisotropic permeability field on one-sided convection has been studied numerically in both two and three dimensions [36,44,112]. These studies show that the broad regimes outlined above remain, but the dynamics and fluxes in each regime are adjusted to reflect the degree of anisotropy. In particular, the statistically constant flux before fingers reach the base of the domain behaves just as in an isotropic medium but with an effective permeability that is the geometric mean $(k_h k_v)^{1/2}$ of the true anisotropic horizontal and vertical permeabilities. In fact, this results also appears to apply to heterogeneous media in some cases: randomly placed horizontal baffles (mimicking common features of geological formations) give a reduction in the mean vertical permeability on a large scale, and the flux appears to respond as though the medium was homogeneous but anisotropic [43,112]. The same results also appear to apply in three dimensions [44].

Other forms of heterogeneity have also been considered: the effect of a thin, low-permeability layer has been the subject of numerical investigation [113], although this study focussed more on the qualitative complexities of how convective dynamics are modulated by such a layer, rather than on understanding and parameterising these effects. Related experimental work in a Hele–Shaw cell [47] used an analogue low-permeability layer that comprised a series of posts across the width of the cell. This study produced some interesting observations, foremost among them that the mean effective permeability of the layer of posts was not the dominant parameter that controlled the flux in this system. Instead, the flux depended on the size of the gaps between posts, and whether their spacing was sufficient to allow thin convective fingers to pass through. These observations are an important reminder of how simple averaging can break down when

[5]There is a slight discrepancy in the predictions of these studies for the limit in which the ideal porous theory should apply. Recasting their different terminology in terms of the Darcy number $Da = k/H^2$, Liang et al. [52] suggest that dispersion is unimportant if $RaDa^{1/2} \ll 1$, which is the constraint given in (2.11), whereas De Paoli et al. [49] suggest that the ideal Hele–Shaw limit will apply if $RaDa \ll 1$. The latter prediction leaves a dependence on the cell height H, which seems unphysical in the context of the one-sided constant-flux regime.

dynamics occur on the same scale as the things that are being averaged, and further experiments in heterogeneous systems would be welcome.

(ii) Geochemistry

There has been a fairly rich vein of relatively recent study looking at the effect of chemical reactions in solutal convection either between the solute and the host medium or between different fluid species present in the medium (see [114] for a comprehensive review of the interplay of chemical reactions with hydrodynamic instabilities). Incorporation of accurate geochemistry into models can be extremely complex, and most modelling approaches have focussed on idealised limits. As well as various studies of the onset problem (e.g. [107,108]), the earlier studies of this problem focussed on the effect of a simple depletion of the dense solute over time owing to chemical reactions (either with another fluid species or with minerals in the fluid matrix), without tracking the change in the other species [115,116]. This idealised scenario has the advantage that the effect of geochemistry can be easily parameterized by a loss term in the transport equation (2.4), and described by a dimensionless Damkohler number, which is typically defined as the product of the reaction rate (with dimensions of $1/\text{time}$) with either the advective or diffusive timescale. In particular, Ward et al. [116] give a detailed overview of the flow dynamics associated with the addition of this new parameter, delineating the different regimes of convection that are possible depending on the relative size of the Rayleigh and Damkohler numbers. The problem can be made sequentially more complicated by keeping track of the concentrations of other species (e.g. [117,118]) or by solving series of coupled reaction-diffusion equations for situations in which multiple species are reacting, which allows for a rich array of possible behaviour (e.g. [119,120], and see [114] for more details).

In the context of reaction with the host medium, some numerical studies have gone beyond these idealised description of the geochemistry to also incorporate evolution of the porosity and permeability of the matrix to reflect precipitation or mineralization of solute [121,122], highlighting the rich array of dynamics and patterns that can arise through the interaction of convective flow and evolving pore-structure of the medium. Many of these studies are motivated by specific applications to CO_2 sequestration, and more accurate modelling of the geochemistry can become extremely complex and dependent on the particular minerals present in the porous rock (e.g. [123]): one has to account for dissolution and precipitation of various species at different rates, and so even simple qualitative questions about whether geochemical reactions enhance or retard convection are not necessarily straightforward to answer. Even without incorporating reactions explicitly, the CO_2-sequestration situation is complicated by the fact that the diffusivity and solubility of gaseous CO_2 depend on the pressure, which can decrease over time as convection proceeds. The one-sided situation discussed here can be adapted to include this effect (e.g. [124,125]), which provides a mechanism to shutdown convection even before the water has become fully saturated.

(iii) Incorporating other dynamics, and applications to CO_2 sequestration

Various studies have extended the ideas of an idealised one-sided setup to describe more realistic flows, motivated, in most cases, by applications in CO_2 sequestration. As outlined in the introduction, supercritical CO_2 injected into a subsurface aquifer is buoyant compared to the ambient water in the pore space under typical reservoir conditions, and so one of the main concerns when injecting it underground is how to keep it there. Suitable aquifers will generally have an effectively impermeable upper boundary or caprock, below which the injected CO_2 will pool and along which it will spread [15]. CO_2 is, however, weakly soluble in water and the resultant CO_2-saturated water is denser than the ambient water. Thus, as injected CO_2 dissolves into water, it becomes dense and can, in principle, lead to downwelling convection, enhanced dissolution, and more secure long-term storage.

Of course, real aquifers have a finite extent, may be sloped or have a complex topography, and may be connected to pre-existing background hydrological flows, and a number of studies

have examined the interaction between one-sided convection and these additional physics. The effect of adding a lateral background flow to the one-sided setup described here was considered by Emami-Meybodi et al. [126], who showed that a sufficiently strong lateral flow can suppress the onset of convection. Szuczewski et al. [127] explored the effect of the geometry of the aquifer in a detailed study focussed on how convection from a dense patch on the upper boundary - mimicking the lateral extent of a CO_2 plume held in a topographic dip - evolves and is eventually shutdown. More recently, some of these ideas were extended to also account for a background hydrological flow in the aquifer [128].

Other studies have focussed on how convection from below an injected patch of CO_2 interacts with the spread of that patch itself under gravity. MacMinn et al. [129] derived a theoretical model to describe how a spreading current of buoyant fluid beneath an impermeable overburden can be gradually arrested by convection from below the current, by incorporating a parameterization of the strength of convection from the work described above. This study was followed by two further experimental studies using quasi-two-dimensional cells filled with bead packs and analogue fluids [130,131] in which this phenomenon was clearly and beautifully observed: convective dissolution from the base of a spreading current can arrest its spread by 'using up' the available fluid. The effect is particularly clear if the cell is tilted so that the current is running upslope [131]. The same behaviour has also been demonstrated and explored in detailed numerical simulations [132].

5. Outlook

This review has attempted to provide an overview of the current state of research into high-Ra convection in fluid-saturated porous media. Convection in general is a phenomenon that has a wide basin of interest: it is a fundamental physical process with countless applications in the earth sciences, engineering and astrophysics, that also exhibits beautiful and complex dynamics and mathematical richness. The aim of this review has been to outline some of these attributes in the case of vigorous porous convection.

There are a number of challenges for future research in the field of high-Ra porous convection. Some of these have already been noted in this review, and some are very briefly discussed in this section; inevitably, different researchers will emphasise different research directions, and so aspects highlighted here may reflect some personal bias. Irrespective of the direction of future research, and despite the fact that this review has focussed on theoretical modelling of convection, it is surely worth noting here the importance of retaining the link between future theoretical or numerical modelling and laboratory experiments or, where possible, field observations and measurements of porous convection. The latter, in particular, are notoriously difficult, since geological convective motion is typically kilometres underground, although some progress is possible by measuring proxies to assess the extend of CO_2 dissolution in aquifers (e.g. [133]) or observing surface features that reflect underground convection patterns (e.g. the patterns in salt deserts [134]).

(a) Heterogeneities and interaction with topography or flow

The interplay of convective flow with heterogeneities or other variations in the porous medium is an interesting problem with open questions. While some previous studies have considered idealised forms of heterogeneity like horizontal layering, the interaction of convection with low-permeability layers has still not been fully explored. One could also imagine sloping or cracked layers affecting convective flow in interesting ways, as might high-permeability lenses or fractures. The effect of many of these heterogeneous features are more complex in three-dimensions, and the interplay of convection with three-dimensional heterogeneity has received very little attention. More broadly, one could consider strong convection in more systematically fractured or cracked matrices using continuum 'bi-porous' models, or the behaviour of thermal

convection when the buoyancy velocity is too fast to allow for thermal equilibrium between the solid matrix and the pore fluid.

(b) Dispersion, pore-scale effects, and the break-down of Darcy's law

Dispersion and its role on convective flow is an active area of research, and there are numerous challenges in this area. As we have seen, various studies have begun to show, at least qualitatively, that dispersion can have a significant effect on convective flows. One challenge is that the manifestation of dispersive behaviour is often rather complex, and it is not always clear how widely one can apply 'simple' continuum parameterisations. Another is that the limit in which mechanical dispersion is the dominant diffusive mechanism is also the limit in which one might expect the construction of pore-averaging that underlies Darcy's law to break down: as discussed in §2(d)iii, we anticipate convective dynamics on lengthscales comparable to the pore scale if the pore-scale Peclet number is large, $\delta_p \hat{u}/D > O(1)$, which is also the limit in which dispersion is believed to be important. Of course, it may be that correctly accounting the for the role of dispersion in this limit helps to alleviate this issue, but nevertheless, the limit in which small plumes becomes of a comparable size to pores is clearly realisable. Promising recent experimental [49] and computational [55] studies have begun to examine these issues in the simpler context of a Hele–Shaw cell, where one can at least rigorously determine the asymptotic corrections associated with a non-infinitesimal gap thickness. Experiments of convection in real porous media that are far from the Darcy limit (i.e. the pore size is very large) [54,84] suggest that convection becomes more like unconfined viscous flow in this limit, but there has been little work in modelling this behaviour. It seems likely that progress in understanding this limit will come from a mixture of experiments, numerical studies in which the pore-scale is fully resolved (cf. [86]) and continuum modelling using extensions of Darcy's law like the Brinkman model or extended Hele–Shaw models (cf. [55]).

In the particular context of convective dissolution of CO_2, there are a number of related challenges that have not been widely considered [135]. CO_2 and water are only partially miscible, and so the complications of two-phase effects, capillarity and relative permeability have a significant effect on the spread of injected CO_2. The implications of these phenomena on convection could be substantial and have not been systematically explored. What effect, for example, does the fact that the 'interface' between water and CO_2 is more likely to be a distributed capillary fringe in which the two phases coexist have on the evolution of convection? A first approximation to this problem has been considered [37], where the capillary fringe was approximated as a region of CO_2 above the interface that was also permeable to brine, and that could be parameterized as a new boundary condition at the interface; I am, however, not aware of studies that extend this initial approximation. An increasing number of impressive direct pore-scale measurements of water and CO_2 in aquifer sandstones (e.g. [136]) show some of the complexity of the water-CO_2 interface at the pore scale, and accurate parameterization of these features in continuum models provides an interesting challenge for the future.

(c) Other convective systems

Of course, high-Ra convection in porous media can arise in more complex settings than those outlined in this review. The Rayleigh–Taylor setup of a dense fluid overlying a buoyant one, for example, has been the subject of a recent numerical study [137]. Internally heated porous convection, driven by a distributed source internal to the medium rather than by a source of buoyancy at a boundary, has recently been suggested as the key hydrological process governing the dynamics of Saturn's moon Enceladus [11] and other astrophysical bodies. Motivated by this application, convection in an idealised internally heated porous medium at high Ra has also been recently studied theoretically and numerically [138].

Convection in a porous medium with an 'open top' - that is, a fixed pressure on one boundary - has been the subject of continued study [5,139,140] because of its relevance to hydrothermal

circulation at mid-ocean ridges. In fact, the fluid mechanics of mid-ocean ridge hydrology are extremely complex (e.g. [6,141]) and contain numerous fascinating modelling challenges for the future, which have yet to be systematically explored and understood. These include accounting for phase change in the medium, accounting for the presence of heat and salt, accurately modelling the boundary between porous and unconfined layers, parameterising highly complex geochemistry and capturing evolution of the pore structure. The first step to understand the qualitative impact of some of these complex phenomena is likely to come from suitable idealised studies in which the key physics are isolated and explored.

Acknowledgements. I am grateful to three anonymous referees for their constructive comments on an earlier draft of this review, and particularly for providing them in the midst of the troubled times of the COVID-19 global emergency.

Funding. DRH was funded by a Research Fellowship at Gonville and Caius College, Cambridge while some of this work was undertaken.

References

1. Ratouis T, Zarrouk S. 2016 Factors controlling large-scale hydrodynamic convection in the TaupoVolcanic Zone (TVZ), New Zealand. *Geothermics* **59**, 236–251.
2. Cheng P. 1978 Heat transfer in geothermal systems. *Adv. Heat Transfer* **14**, 1–105.
3. Stein C. 1995 Heat flow of the Earth. In *Global Earth physics: a handbook of physical constants*,. AGU.
4. Davis E, Wang K, He J, Chapman D, Villinger H, Rosenberger A. 1997 An unequivocal case for high Nusselt number hydrothermal convection in sediment-buried igneous oceanic crust. *Earth Planetary Sci. Lett.* **146**, 137–150.
5. Cherkaouim A, Wilcock W. 1999 Characteristics of high Rayleigh number two-dimensional convection in an open-top porous layer heated from below. *J. Fluid Mech.* **394**, 241–260.
6. Ingebritsen S, Geiger S, Hurwitz S, Driesner T. 2010 Numerical simulation of magmatic hydrothermal systems. *Rev. Geophys.* **48**, RG1002.
7. Wooding R, Tyler S, White I. 1997a Convection in groundwater below an evaporating salt lake: 1. Onset of instability. *Water Resour. Res.* **33**, 1199 – 1217.
8. Wooding R, Tyler S, White I, Anderson P. 1997b Convection in groundwater below an evaporating salt lake: 2. Evolution of fingers or plumes. *Water Resour. Res.* **33**, 1219–1228.
9. Wilson A, Ruppel C. 2007 Salt tectonics and shallow subseafloor fluid convection: models of coupled fluid-heat-salt transport. *Geofluids* **7**, 377–386.
10. Notz D, Worster M. 2009 Desalination processes of sea ice revisited. *J. Geophys. Res.* **114**, C05006.
11. Choblet G, Tobie G, Sotin C, Běhounková M, Čadek O, Postberg F, Souček O. 2017 Powering prolonged hydrothermal activity inside Enceladus. *Nature Astron.* **1**, 841–847.
12. Bachu S. 2008 CO_2 storage in geological media: role, means, status and barriers to deployment. *Prog. Ener. Combust. Sci.* **34**, 254–273.
13. Orr Jr. F. 2009 Onshore Geologic storage of CO_2. *Science* **325**, 1656 – 1658.
14. Bickle M. 2009 Geological carbon storage. *Nature Geosci.* **2**, 815–819.
15. Huppert HE, Neufeld JA. 2014 The fluid mechanics of carbon dioxide sequestration. *Ann. Rev. Fluid Mech.* **46**, 255–272.
16. Emami-Maybodi H, Hassanzadeh H, Green C, Ennis-King J. 2015 Convective dissolution of CO_2 in saline aquifers: Progress in modelingand experiments. *Int. J. Greenhouse Gas Control* **40**, 238–266.
17. Metz B, Davidson O, de Coninck H, Loos M, Meyer L. 2005 *IPCC Special Report on Carbon Dioxide Capture and Storage*. CUP.
18. Turner J. 1973 *Buoyancy effects in fluids*. CUP.
19. Linden P. 2000 6: Convection in the Environment. In *Perspectives in Fluid Dynamics*,. CUP.
20. Nield D, Bejan A. 2017 *Convection in Porous media*. Springer fifth edition.
21. Siggia E. 1994 High Rayleigh number convection. *Ann. Rev. Fluid Mech.* **26**, 137–168.
22. Ahlers G, Grossmann S, Lohse D. 2009 Heat transfer and large scale dynamics in turbulent Rayleigh-Bénard convection. *Rev. Mod. Phys.* **81**, 503–537.
23. Bear J. 1988 *Dynamics of Fluids in porous Media*. Dover.
24. Phillips O. 2009 *Geological Fluids Dynamics*. CUP.

25. Banu N, Rees D. 2002 Onset of Darcy–Benard convection using a thermalnon-equilibrium model. *Int. J. Heat Mass Transfer* **45**, 2221–2228.
26. Rees D, Pop I. 2005 6: Local thermal non-equilibrium in porous medium convection. In *Transport Phenomena in Porous Media*, vol. III, . Elsevier.
27. Straughan B. 2006 Global nonlinear stability in porous convection with a thermal non-equilibrium model. *Proc. R. Soc. A* **462**, 409–418.
28. Landman A, Schotting R. 2007 Heat and brine transport in porous media: the Oberbeck-Boussinesq approximation revisited. *Transp. Porous Media* **70**, 355–373.
29. Nield D, Kuznetsov A. 2006 The onset of convection in a bidisperse porous medium. *Int. J. Heat Mass Transfer* **49**, 3068–3074.
30. Nield D. 2016 A note on the modelling of bidisperse porous media. *Transp. Porous Media* **111**, 517–520.
31. Straughan B. 2018 Horizontally isotropic bidispersive thermal convection. *Proc. R. Soc. A* **474**, 20180018.
32. Bijeljic B, Blunt B. 2007 Pore-scale modeling of transverse dispersion in porous media. *Water Resour. Res.* **43**, W12S11.
33. Woods A. 2015 *Flow in porous rocks*. CUP.
34. Hewitt D, Lister J. 2017 Stability of columnar convection in a three-dimensional porous medium. *J. Fluid Mech.* **829**, 89–111.
35. Wen B, Corson L, Chini G. 2015 Structure and stability of steady porous medium convection at large Rayleigh number. *J. Fluid Mech.* **772**, 197–224.
36. De Paoli M, Zonta F, Soldati A. 2017 Dissolution in anisotropic porous media: Modelling convection regimes from onset to shutdown. *Phys. Fluids* **29**, 026601.
37. Slim A. 2014 Solutal convection regimes in a two-dimensional porous medium. *J. Fluid Mech.* **741**, 461–491.
38. Otero J, Dontcheva L, Johnston H, Worthing R, Kurganov A, Petrova G, Doering C. 2004 High-Rayleigh-number convection in a fluid-saturated porous layer. *J. Fluid Mech.* **500**, 263–281.
39. Hewitt D, Neufeld J, Lister J. 2012 Ultimate Regime of High Rayleigh number convection in a porous medium. *Phys. Rev. Lett.* **108**, 224503.
40. Hidalgo J, Fe J, Cueto-Felgueroso L, Juanes R. 2012 Scaling of convective mixing in porous media. *Phys. Rev. Lett.* **109**, 264503.
41. Hewitt D, Neufeld J, Lister J. 2013 Convective shutdown in a porous medium at high Rayleigh number. *J. Fluid Mech.* **719**, 551–586.
42. Fu X, Cueto-Felgueroso L, Juanes R. 2013 Pattern formation and coarsening dynamics in three-dimensional convective mixing in porous media. *Phil. Trans. R. Soc. A* **371**, 20120355.
43. Elenius M, Gasda S. 2013 Convective mixing in formations with horizontal barriers. *Adv. Water Resour.* **62**, 499–510.
44. Green C, Ennis-King J. 2018 Steady Flux Regime During Convective Mixing in Three-Dimensional Heterogeneous Porous Media. *Fluids* **3**, 58.
45. Backhaus S, Turitsyn K, Ecke R. 2011 Convective Instability and Mass Transport of Diffusion Layers in a Hele-Shaw Geometry. *Phys. Rev. Lett.* **106**, 104501.
46. Ecke R, Backhaus S. 2016 Plume dynamics in Hele-Shaw porous media convection. *Phil. Trans. R. Soc. A* **374**, 20150420.
47. Salibindla A, Subedi R, Shen V, Masuk A, Ni R. 2018 Dissolution-driven convection in a heterogeneous porous medium. *J. Fluid Mech.* **857**, 61–79.
48. Slim A, Bandi M, Miller J, Mahadevan L. 2013 Dissolution-driven convection in a Hele-Shaw cell. *Phys. Fluids* **25**, 024101.
49. De Paoli M, Alipour M, Soldati A. 2020 How non-Darcy effects influence scaling laws in Hele-Shaw convection experiment. *J. Fluid Mech.* **in press**.
50. Elder J. 1967 Steady free convection in a porous medium heated from below. *J. Fluid Mech.* **27**, 29–48.
51. Neufeld J, Hesse M, Riaz A, Hallworth M, Tchelepi H, Huppert H. 2010 Convective dissolution of carbon dioxide in saline aquifers. *Geophys. Res. Lett.* **37**, 22404.
52. Liang Y, Wen B, Hesse M, DiCarlo D. 2018 Effect of Dispersion on Solutal Convection in Porous Media. *Geophys. Res. Lett.* **45**, 9690–9698.
53. Lister C. 1990 An explanation for the multivalued heat transport found experimentally for convection in a porous medium. *J. Fluid Mech.* **214**, 287–320.
54. Keene D, Goldstein R. 2015 Thermal convection in Porous media at high Rayleigh numbers. *J. Heat Transfer* **137**, 034503.

55. Letelier J, Mujica N, Ortega J. 2019 Perturbative corrections for the scaling of heat transport in a Hele-Shaw geometry and its application to geological vertical fractures. *J. Fluid Mech.* **864**, 746–767.
56. Jha B, Cueto-Felgueroso L, Juanes R. 2011 Fluid Mixing from Viscous Fingering. *Phys. Rev. Lett.* **106**, 194502.
57. Lapwood E. 1948 Convection of a fluid in a porous medium. *Math. Proc. Cam. Phil. Soc.* **44**, 508–521.
58. Robinson J, O'Sullivan M. 1976 A boundary-layer model of flow in a porous medium at high Rayleigh number. *J. Fluid Mech.* **75**, 459–467.
59. Kimura S, Schubert G, Strauss J. 1986 Route to chaos in porous-medium thermal convection. *J. Fluid Mech.* **166**, 305–324.
60. Graham M, Steen P. 1994 Plume formation and resonant bifurcations in porous-media convection. *J. Fluid Mech.* **272**, 67–89.
61. Hewitt D, Neufeld J, Lister J. 2014 High Rayleigh number convection in a three-dimensional porous medium. *J. Fluid Mech.* **748**, 879–895.
62. Malkus W. 1954 Discrete Transitions in turbulent convection. *Proc. R. Soc. Lond. A* **225**, 185–195.
63. Howard L. 1964 Convection at High Rayleigh number. In Görtler H, editor, *Applied Mechanics, Proc. 11th Intl Cong. Appl. Math.* pp. 1109–1115.
64. Kraichnan R. 1962 Turbulent Thermal Convection at arbitrary Prandtl number. *Phys. Fluids* **5**, 1374–1389.
65. Spiegel E. 1971 Convection in stars I. Basic Boussinesq convection. *Annu. Rev. Astron. Astr.* **9**, 323.
66. Iyer K, Scheel JD, Schumacher J, Sreenivasan K. 2020 Classical 1/3 scaling of convection holds up to $Ra = 10^{15}$. *PNAS* **117**, 7594–7598.
67. Busse F, Joseph D. 1972 Bounds for heat transport in a porous layer. *J. Fluid Mech.* **54**, 521–543.
68. Gupta V, Joseph D. 1973 Bounds for heat transport in a porous layer. *J. Fluid Mech.* **57**, 491 – 514.
69. Howard L. 1972 Bounds on flow quantites. *Ann. Rev. Fluid Mech.* **4**, 473–494.
70. Doering C, Constantin P. 1996 Variational bounds on energy dissipation in incompressible flows: III. Convection. *Phys. Rev. E* **53**, 5957–5981.
71. Wen B, Dianati N, Lunasin E, Chini G, Doering C. 2012 New upper bounds and reduced dynamical modeling for Rayleigh-Bénard convection in a fluid-saturated porous layer. *Commun. Nonlinear Sci. Numerical Sim.* **17**, 2191–2199.
72. Wen B, Chini G, Dianati N, Doering C. 2013 Computational approaches to aspect-ratio-dependent upper bounds and heat flux in porous medium convection. *Phys. Lett. A* **377**, 2931–2938.
73. De Paoli M, Zonta F, Soldati A. 2016 Influence of anisotropic permeability on convection in porous media: Implications for geological CO_2 sequestration. *Phys. Fluids* **28**, 056601.
74. Hewitt D, Neufeld J, Lister J. 2013 Stability of columnar convection in a porous medium. *J. Fluid Mech.* **737**, 205–231.
75. Caltagirone J, Bories S. 1985 Solutions and stability criteria of natural convective flow in an inclined porous layer. *J. Fluid Mech.* **155**, 267–287.
76. Rees D, Bassom A. 2000 The onset of Darcy–Bénard convection in an inclined layer heated from below. *Acta Mech.* **144**, 103–118.
77. Voss C, Simmons C, Robinson N. 2010 Three-dimensional benchmark for variable-density flow and transport simulation: matching semi-analytic stability modes for steady unstable convection in an inclined porous box. *Hydrogeology J.* **18**, 5–23.
78. Wen B, Chini G. 2018 Inclined porous medium convection at large Rayleigh number. *J. Fluid Mech.* **837**, 670–702.
79. Hewitt D, Neufeld J, Lister J. 2014 High Rayleigh number convection in a porous medium containing a thin low-permeability layer. *J. Fluid Mech.* **756**, 844–869.
80. McKibbin R, Tyvand P. 1983 Thermal convection in a porous medium composed of alternating thick and thin layers. *Int. J. Heat Mass Transfer* **26**, 761–780.
81. Nakanishi Y, Hyodo A, Wang L, Suekane T. 2016 Experimental study of 3D Rayleigh–Taylor convection between miscible fluids in a porous medium. *Adv. Water Resour.* **97**, 224–232.
82. Wang L, Nakanishi Y, Hyodo A, Suekane T. 2016 Three-dimensional structure of natural convection in a porous medium: Effect of dispersion on finger structure. *Int. J. Greenhouse Gas Control* **53**, 274–283.

83. Wen B, Chang K, Hesse M. 2018 Rayleigh–Darcy convection with hydrodynamic dispersion. *Phys. Rev. Fluids* **3**, 123801.
84. Ataei-Dadavi I, Chakkingal M, Kenjeres S, Kleijn C, Tummers M. 2019 Flow and heat transfer measurements in natural convection in coarse-grained porous media. *Int. J. Heat Mass Transfer* **130**, 575–584.
85. Vishnampet R, Narasimhan A, Babu V. 2011 High Rayleigh Number Natural Convection inside 2D porous enclosures using the Lattice Boltzmann Method. *J. Heat Transfer* **133**, 062501.
86. Gasow S, Lin Z, Zhang H, Kuznetsov A, Avila M, Jin Y. 2020 Effects of pore scale on the macroscopic properties of natural convection in porous media. *J. Fluid Mech.* **891**, A25.
87. Holzer M, Siggia E. 1994 Turbulent mixing of a passive scalar. *Phys. Fluids* **6**, 1820.
88. Jenny P, Lee J, Meyer D, Tchelepi H. 2014 Scale analysis of miscible density-driven convection in porous media. *J. Fluid Mech.* **749**, 519–541.
89. Ennis-King J, Paterson L. 2005 Role of convective mixing in the long-term storage of carbon dioxide in deep saline formations. *SPE J.* **10**, 349–356.
90. Slim A, Ramakrishnan T. 2010 Onset and cessation of time-dependent, dissolution-driven convection in porous media. *Phys. Fluids* **22**, 124103.
91. Caltagirone J. 1980 Stability of a saturated porous layer subject to a sudden rise in surface temperature: comparison between the linear and energy methods. *Q. J. Mech. Appl. Math.* **33**, 47–58.
92. Riaz A, Hesse M, Tchelepi H, Orr Jr. F. 2006 Onset of convection in a gravitationally unstable diffusive layer in porous media. *J. Fluid Mech.* **548**, 87–111.
93. Xu X, Chen S, Zhang Z. 2006 Convective stability analysis of the long-term storage of carbon dioxide in deep saline aquifers. *Adv. Water Resour.* **29**, 397–497.
94. Rapaka S, Chen S, Pawar R, Stauffer P, Zhang D. 2008 Non-modal growth of perturbations in density-driven convection in porous media. *J. Fluid Mech.* **609**, 285–303.
95. Kim M, Choi C. 2012 Linear stability analysis on the onset of buoyancy-driven convection in liquid- saturated porous medium. *Phy. Fluids* **24**, 044102.
96. Daniel D, Tilton N, Riaz A. 2013 Optimal perturbations of gravitationally unstable transient boundary layers in porous media. *J. Fluid Mech.* **727**, 456–487.
97. Tilton N, Daniel D, Riaz A. 2013 The initial transient period of gravitationally unstable diffusive boundary layers developing in porous media. *Phys. Fluids* **25**, 092107.
98. Tilton N, Riaz A. 2014 Nonlinear stability of gravitationally unstable, transient, diffusive boundary layers in porous media. *J. Fluid Mech.* **745**, 251–278.
99. Tilton N. 2018 Onset of transient natural convection in porous media due to porosity perturbations. *J. Fluid Mech.* **838**, 129–147.
100. Kim M, Choi C. 2011 The stability of miscible displacement in porous media: Nonmonotonic viscosity profiles. *Phys. Fluids* **23**, 084105.
101. Daniel D, Riaz A. 2014 Effect of viscosity contrast on gravitationally unstable diffusive layers in porous media. *Phys. Fluids* **26**, 116601.
102. Raad S, Hassanzadeh H. 2015 Onset of dissolution-driven instabilities in fluids with nonmonotonic density profile. *Phys. Rev. E* **92**, 053023.
103. Hidalgo J, Carrera J. 2009 Effect of dispersion on the onset of convection during CO_2 sequestration. *J. Fluid Mech.* **640**, 441–452.
104. Rapaka S, Pawar R, Stauffer P, Zhang D, Chen S. 2009 Onset of convection over a transient base-state in anisotropic and layer porous media. *J. Fluid Mech.* **641**, 227–244.
105. Daniel D, Riaz A, Tchelepi H. 2015 Onset of natural convection in layered aquifers. *J. Fluid Mech.* **767**, 763–781.
106. Daniel D. 2017 Convective mixing in vertically-layered porous media: The linear regime and the onset of convection. *Phys. Fluids* **29**, 084101.
107. Andres J, Cardoso S. 2011 Onset of convection in a porous medium in the presence of chemical reaction. *Phys. Rev. E* **83**, 046312.
108. Ward T, Cliffe K, Jensen O, Power H. 2014 Dissolution-driven porous-medium convection in the presence of chemical reaction. *J. Fluid Mech.* **747**, 316–349.
109. Pau G, Bell J, Pruess K, Almgren A, Lijewski M, Zhang K. 2010 High-resolution simulation and characterization of density-driven flow in CO_2 storage in saline aquifers. *Adv. Water Resour.* **33**, 443–455.
110. Tsai.P.A., Riesing K, Stone HA. 2013 Density-driven convection enhanced by an inclined boundary: Implications for geological CO_2 storage. *Phys. Rev. E* **87**, 011003.

111. Ghesmat K, Hassanzadeh H, Abedi J. 2011 The effect of anisotropic dispersion on the convective mixing in long-term CO_2 storage in saline aquifers. *AIChE Journal* **57**, 561–570.
112. Green C, Ennis-King J. 2014 Steady dissolution rate due to convective mixing in anisotropic porous media. *Adv. Water Resour.* **73**, 65–73.
113. Soboleva E. 2018 Density-driven convection in an inhomogeneous geothermal reservoir. *Int. J. Heat Mass Transfer* **127**, 784–798.
114. De Wit A. 2020 Chemo-Hydrodynamic patterns and instabilities. *Ann. Rev. Fluid Mech.* **52**, 531–555.
115. Andres J, Cardoso S. 2012 Convection and reaction in a diffusive boundary layer in a porous medium: Nonlinear dynamics. *Chaos* **22**, 037113.
116. Ward T, Jensen O, Power H, Riley D. 2014 High-Rayleigh-number convection of a reactive solute in a porous medium. *J. Fluid Mech.* **760**, 95–126.
117. Ennis-King J, Paterson L. 2007 Coupling of geochemical reactions and convective mixing in the long-term geological storage of carbon dioxide. *Int. J. Greenhouse Gas Control* **1**, 86–93.
118. Ghesmat K, Hassanzadeh H, Abedi J. 2011 The impact of geochemistry on convective mixing in a gravitationally unstable diffusive boundary layer in porous media: CO_2 storage in saline aquifers. *J. Fluid Mech.* **673**, 480–512.
119. Loodts V, Thomas C, Rongy L, De Wit A. 2014 Control of Convective Dissolution by Chemical Reactions: General Classification and Application to CO_2 Dissolution in Reactive Aqueous Solutions. *Phys. Rev. Lett.* **113**, 114501.
120. Kim M, Cardoso S. 2018 Diffusivity ratio effect on the onset of the buoyancy-driven instability of an $A + B \implies C$ chemical reaction system in a Hele-Shaw cell: asymptotic and linear stability analyses. *Phys. Fluids* **30**, 094102.
121. Hidalgo J, Dentz M, Cabeza Y, Carrera J. 2015 Dissolution patterns and mixing dynamics in unstable reactive flow. *Geophys. Res. Lett.* **42**, 6357 – 6364.
122. Fu X, Cueto-Felgueroso L, Bolster D, Juanes R. 2015 Rock dissolution patterns and geochemical shutdown of CO_2-brine-carbonate reactions during convective mixing in porous media. *J. Fluid Mech.* **764**, 296–315.
123. Sainz-Garcia A, Abarca E, Nardi A, Grandia F, Oelkers E. 2017 Convective mixing fingers and chemistry interaction in carbon storage. *Int. J. Greenhouse Gas Control* **58**, 52–61.
124. Wen B, Akhbari D, Zhang L, Hesse M. 2018 Convective carbon dioxide dissolution in a closed porous medium at low pressure. *J. Fluid Mech.* **854**, 56–87.
125. Shi Z, Wen B, Hesse M, Tsotsis T, Jessen K. 2018 Measurement and modeling of CO_2 mass transfer in brine at reservoir conditions. *Adv. Water Resour.* **113**, 100–111.
126. Emami-Maybodi H, Hassanzadeh H, Ennis-King J. 2015 CO_2 dissolution in the presence of background flow of deep saline aquifers. *Water Resour. Res.* **51**, 2595–2615.
127. Szulczewski M, Hesse M, Juanes R. 2013 Carbon dioxide dissolution in structural and stratigraphic traps. *J. Fluid Mech.* **736**, 287–315.
128. Unwin H, Wells G, Woods A. 2016 CO_2 dissolution in a background hydrological flow. *J. Fluid Mech.* **789**, 768–784.
129. MacMinn C, Szulczewski M, Juanes R. 2011 CO_2 migration in saline aquifers: regimes in migration with dissolution. *Energy Proc.* **4**, 3904–3910.
130. MacMinn C, Neufeld JA, Hesse M, Huppert H. 2012 Spreading and convective dissolution of carbon dioxide in vertically confined, horizontal aquifers. *Water Resour. Res.* **48**, W11516.
131. MacMinn C, Juanes R. 2013 Buoyant currents arrested by convective dissolution. *Geophys. Res. Lett.* **40**, 2017–2022.
132. Hidalgo J, MacMinn C, Juanes R. 2013 Dynamics of convective dissolution from a migrating current of carbon dioxide. *Adv. Water Resour.* **62**, 511–519.
133. Bickle MJ, Kampman N. 2013 Lessons in carbon storage from geological analogues. *Geology* **41**, 525–526.
134. Lasser J, Nield J, Ernst M, Karius V, Wiggs G, Goehring L. 2019 Salt polygons are caused by convection. *arXiv:1902.03600*.
135. Bui M, Adjiman CS, Bardow A, Anthony EJ, Boston A, Brown S, Fennell PS, Fuss S, Galindo A, Hackett LA, Hallett JP, Herzog HJ, Jackson G, Kemper J, Krevor S, Maitland GC, Matuszewski M, Metcalfe IS, Petit C, Puxty G, Reimer J, Reiner DM, Rubin ES, Scott SA, Shah N, Smit B, Trusler JPM, Webley P, Wilcox J, Mac Dowell N. 2018 Carbon capture and storage (CCS): the way forward. *Energy & Environmental Science* **11**, 1062–1176.
136. Krevor SCM, Pini R, Zuo L, Benson S. 2012 Relative permeability and trapping of CO_2 and water in sandstone rocks at reservoir conditions. *Water Resour. Res.* **48**, W02532.

137. De Paoli M, Zonta F, Soldati A. 2019 Rayleigh-Taylor convective dissolution in confined porous media. *Phys. Rev. Fluids* **4**, 023502.
138. Le Reun T, Hewitt D. 2020 Internally heated porous convection: an idealised model for Enceladus' hydrothermal activity. *Geophys. J. Int.* **under review**.
139. Rabinowicz M, Boulegue J, Genthon P. 1998 Two- and three-dimensional modeling of hydrothermal convection in the sedimented Middle Valley degment, Juan de Fuca Ridge. *J. Geophys. Res.* **103**, 24045.
140. Fontaine F, Wilcock W. 2017 Two-dimensional numerical models of open-top hydrothermal convection at high Rayleigh and Nusselt numbers: Implications for mid-ocean ridge hydrothermal circulation. *Geochem., Geophys., Geosyst.* **8**, Q07010.
141. Schoofs S, Hansen U. 2000 Depletion of a brine layer at the base of ridge-crest hydrothermal systems. *Earth Planetary Sci. Lett.* **180**, 341–353.